



UNIVERSITY OF GOTHENBURG

An edited version of this paper was published by AGU. Copyright (2016) American Geophysical Union.

Citation for the published paper:

Andrén, M., G. Stockmann, A. Skelton, E. Sturkell, C.-M. Mörth, H. R. Guðrúnardóttir, N. S. Keller, N. Odling, B. Dahrén, C. Broman, et al. (2016), Coupling between mineral reactions, chemical changes in groundwater, and earthquakes in Iceland, *J. Geophys. Res. Solid Earth*, 121, 2315–2337, doi:10.1002/2015JB012614.

GUP

Gothenburg University Publications

<http://gup.ub.gu.se>

RESEARCH ARTICLE

10.1002/2015JB012614

Coupling between mineral reactions, chemical changes in groundwater, and earthquakes in Iceland

Key Points:

- Eight years of groundwater monitoring records changes before and after $M > 5$ earthquakes
- Long-term chemical changes can be explained by stoichiometric replacement of plagioclase by analcime and zeolites
- Short-term chemical changes associated with earthquakes can be explained by nonstoichiometric release of Na from analcime

Supporting Information:

- Supporting Information S1
- Data Set S1
- Data Set S2

Correspondence to:

G. Stockmann,
gabrielle.stockmann@geo.su.se

Citation:

Andr n, M., et al. (2016), Coupling between mineral reactions, chemical changes in groundwater, and earthquakes in Iceland, *J. Geophys. Res. Solid Earth*, 121, 2315–2337, doi:10.1002/2015JB012614.

Received 20 OCT 2015

Accepted 20 MAR 2016

Accepted article online 25 MAR 2016

Published online 9 APR 2016

Margareta Andr n¹, Gabrielle Stockmann¹, Alasdair Skelton¹, Erik Sturkell², Carl-Magnus M rth¹, Helga Raket Gu r nard ttir¹, Nicole Simone Keller³, Nic Odling⁴, B rje Dahr n⁵, Curt Broman¹, Tonci Balic-Zunic⁶, Hreinn Hjartarson⁷, Heike Siegmund¹, Friedemann Freund⁸, and Ingrid Kockum⁹

¹Department of Geological Sciences, Stockholm University, Stockholm, Sweden, ²Department of Earth Sciences, University of Gothenburg, Gothenburg, Sweden, ³Institute of Earth Sciences, University of Iceland, Reykjav k, Iceland, ⁴School of Geosciences, University of Edinburgh, Edinburgh, Scotland, ⁵Department of Earth Sciences, Uppsala University, Uppsala, Sweden, ⁶Natural History Museum, University of Copenhagen, Copenhagen, Denmark, ⁷Landsvirkjun, Reykjav k, Iceland, ⁸NASA Ames Research Center, Earth Science Division, Moffett Field, California, USA, ⁹Karolinska Institutet, Stockholm, Sweden

Abstract Chemical analysis of groundwater samples collected from a borehole at Hafral kur, northern Iceland, from October 2008 to June 2015 revealed (1) a long-term decrease in concentration of Si and Na and (2) an abrupt increase in concentration of Na before each of two consecutive $M > 5$ earthquakes which occurred in 2012 and 2013, both 76 km from Hafral kur. Based on a geochemical (major elements and stable isotopes), petrological, and mineralogical study of drill cuttings taken from an adjacent borehole, we are able to show that (1) the long-term decrease in concentration of Si and Na was caused by constant volume replacement of labradorite by analcime coupled with precipitation of zeolites in vesicles and along fractures and (2) the abrupt increase of Na concentration before the first earthquake records a switchover to nonstoichiometric dissolution of analcime with preferential release of Na into groundwater. We attribute decay of the Na peaks, which followed and coincided with each earthquake to uptake of Na along fractured or porous boundaries between labradorite and analcime crystals. Possible causes of these Na peaks are an increase of reactive surface area caused by fracturing or a shift from chemical equilibrium caused by mixing between groundwater components. Both could have been triggered by preseismic dilation, which was also inferred in a previous study by Skelton et al. (2014). The mechanism behind preseismic dilation so far from the focus of an earthquake remains unknown.

1. Introduction

Since the 1960s there have been numerous reports of changes in groundwater chemistry before and after earthquakes. These include variations in radon count rates [Wakita, 1981; Hauksson and Goddard, 1981; Wakita et al., 1991; Wakita, 1996; Igarashi et al., 1995], concentrations of sulphate and chloride ions [Wakita, 1996; Song et al., 2006], concentrations of transition metals [Claesson et al., 2004], concentrations of Na, Si, and Ca [Claesson et al., 2007; W steb y et al., 2014; Skelton et al., 2014], and stable isotope ratios [Reddy et al., 2011; Skelton et al., 2014]. Whereas most researchers agree that changes of groundwater chemistry occur after earthquakes, no such consensus exists regarding changes of groundwater chemistry before earthquakes (hydrochemical precursors). The precursory changes reported in the literature range in time and length scales from 1 day to 6 months and from 5 to 400 km, respectively [Wakita, 1981; Hauksson and Goddard, 1981; Wakita et al., 1991; Tsunogai and Wakita, 1995; Igarashi et al., 1995; Song et al., 2006; Claesson et al., 2004; Yaman et al., 2011; Skelton et al., 2014]. The reason that precursory signals are often questioned is that (1) most studies of hydrochemical precursors have failed to rule out explanations unrelated to earthquakes, (2) reproducibility of precursory signals has seldom been shown, and (3) few precursors have been validated statistically [Roeloffs, 1988; Wang and Manga, 2010; Ingebritsen and Manga, 2014]. One exception is a recent study conducted by Skelton et al. [2014] in a part of northern Iceland which is presently undergoing a prolonged period of seismic quiescence and therefore at elevated risk for M 6–7 earthquakes. These authors reported changes of $\delta^2\text{H}$ values and Na concentration in Ice Age groundwater before two consecutive earthquakes. The first of these earthquakes was on 21 October 2012 (M 5.6), and the second earthquake was on 2 April 2013 (M 5.3). Groundwater samples were taken from ground level of a borehole at Hafral kur, which is located 30 km from H sav k and 76 km from the epicenters of both earthquakes (Figure 1). Using a

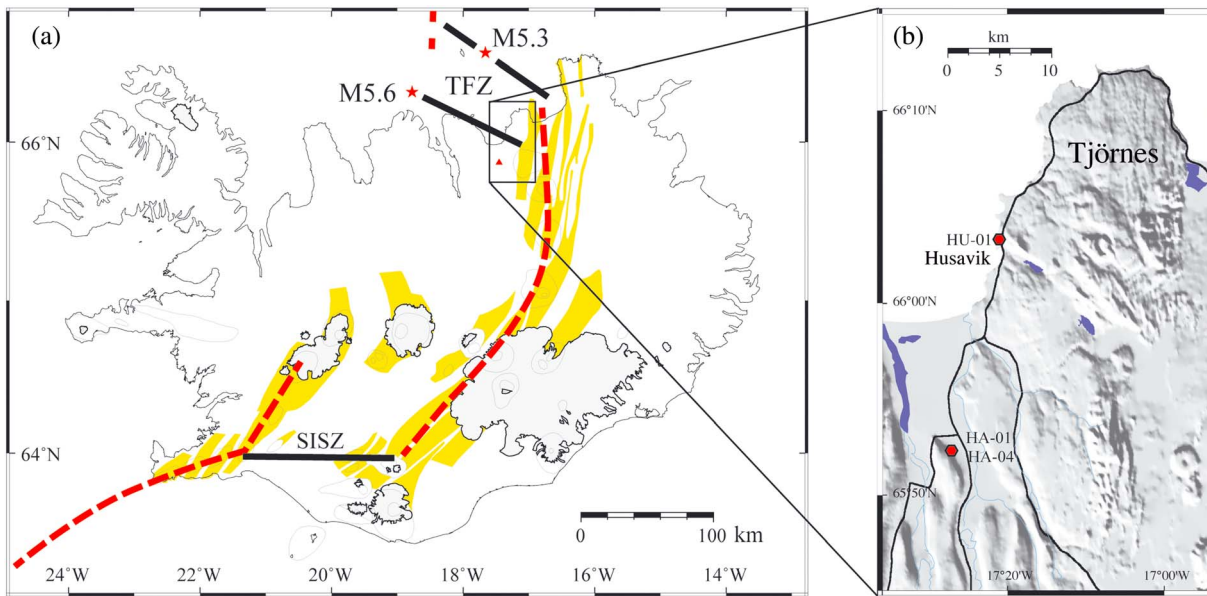


Figure 1. (a) Map of Iceland showing the Mid-Atlantic Ridge passing through the volcanic island, separating the American plate from the Eurasian plate. The divergent plate boundary is shown with red dashed lines and the Transform Zones (SISZ and TFZ) with black lines. Yellow areas mark the active volcanic systems from *Einarsson and Sæmundsson* [1987]. Two earthquakes $M > 5$ reported in *Skelton et al.* [2014] are represented by star symbols. (b) Zoom in of the study area (Tjörnes peninsula) where the boreholes HA-01 and HA-04 are located. The location of borehole HU-01, which was studied by *Wästeby et al.* [2014], is shown for reference.

binomial test, *Skelton et al.* [2014] were able to demonstrate probable association of these hydrochemical precursory signals with both earthquakes (p value = 10^{-5}). They attributed this association to mixing of groundwater components in response to crustal dilation, a mechanism put forward previously to explain precursory phenomena [*Scholz et al.*, 1973; *Thomas*, 1988]. This interpretation was motivated by observed increases of $\delta^2\text{H}$ from an average baseline value of -126.6 ± 2.7 ‰ to maxima of -122.0 ± 0.6 ‰ and -120.2 ± 0.6 ‰ before the earthquakes [*Skelton et al.*, 2014]. These increases are too large to be explained by isotopic fractionation associated with water-rock interaction at the observed timescale of months and more likely reflect an influx of modern day groundwater, which is isotopically heavier ($\delta^2\text{H} \sim -70$ ‰).

Skelton et al. [2014] further pointed out that the increase of Na concentration observed in their study might reflect a different mechanism. In a study of groundwater samples taken from a borehole in Húsavík (Figure 1), *Claesson et al.* [2007] and *Wästeby et al.* [2014] showed that Na as well as several other elements, e.g., Si and Ca, was mainly acquired by water-rock interaction on a timescale of decades. *Claesson et al.* [2007] further showed that water-rock interaction on this timescale was accompanied by an increase of $\delta^{18}\text{O}$. This is expected because the $\delta^{18}\text{O}$ value of the basaltic host rock is ≥ 5 ‰, which is far heavier than for Ice Age groundwater at Hafnalækur where $\delta^{18}\text{O}$ values range from -18 to -15 ‰. The modern day groundwater, responsible for the precursory $\delta^2\text{H}$ increases at Hafnalækur, has had a comparatively short time to undergo water-rock interaction, and thus, an influx of this groundwater is unlikely to have caused the observed increase of the concentration of Na. Also, no concomitant increase of $\delta^{18}\text{O}$ was observed [*Skelton et al.*, 2014].

The aim of this study is to explore the mechanisms behind observed changes of Na concentration in groundwater at Hafnalækur. Our strategy is to conduct a petrological, mineralogical, and geochemical study of drill cuttings, which were taken from a second borehole, which is alongside the one from which groundwater samples are taken. Our purpose is to further our understanding of the mechanism, whereby elements are released to and removed from groundwater at Hafnalækur, so as to explain longer-term variation of groundwater chemistry during our measurement campaign as well as short-term changes (Na peaks) that coincided with the earthquakes.

2. Geological Background

The tectonic setting of Iceland is dominated by an eastward shift of the Mid-Atlantic Ridge because of a hot spot currently located under Vatnajökull in SE Iceland. This has created two parallel transform zones: the

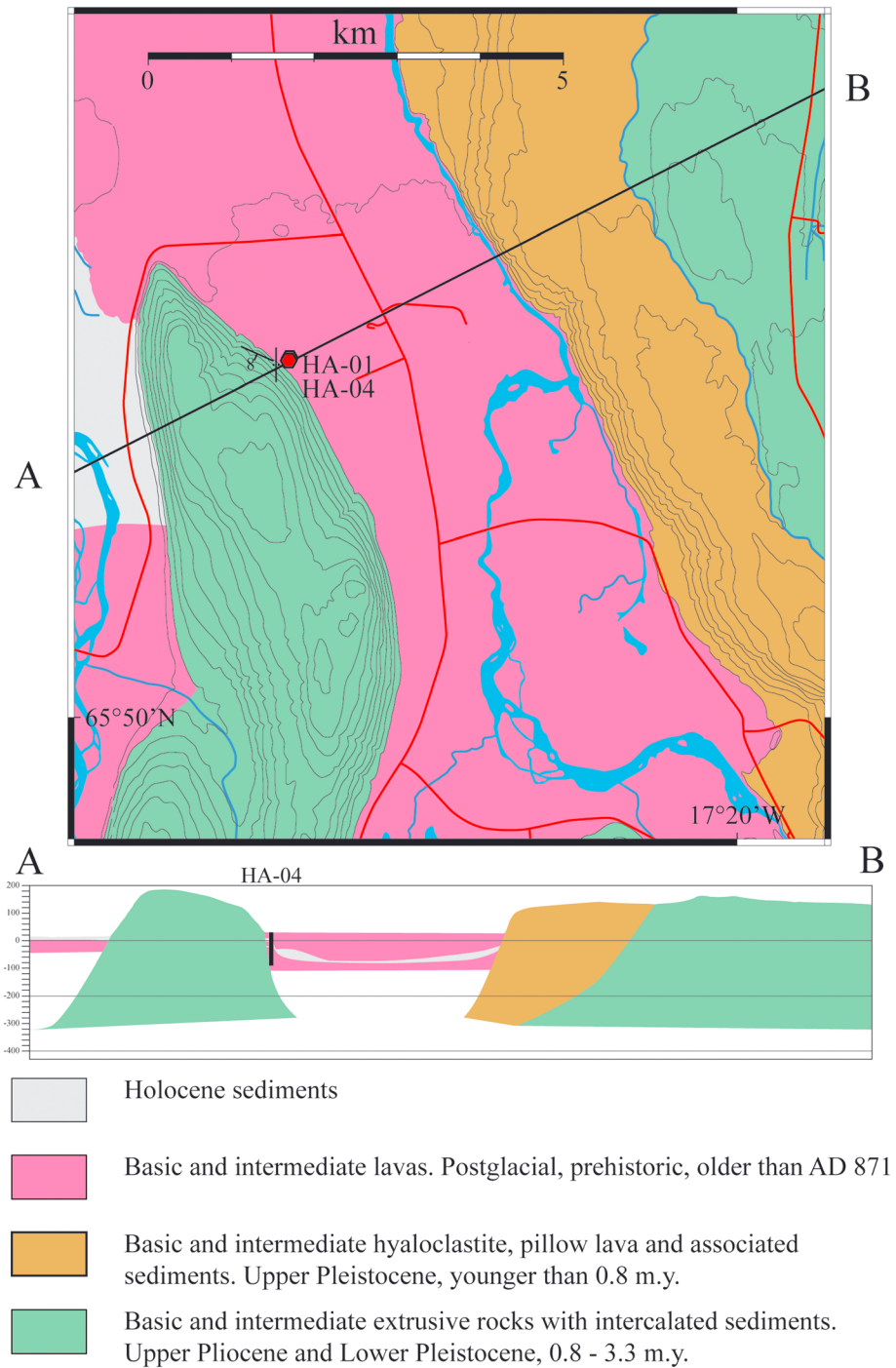


Figure 2. Geological map based on *Johannesson and Saemundsson* [2009] and cross section of the area around Hafnalækur. Boreholes HA-01 and HA-04 penetrate postglacial lavas (pink). The grey layer in the cross section (Holocene sediments) is a high-permeability layer, which was identified by resistivity measurements. This is likely to represent the position of the main aquifer at the time of measurement. The profile is based on drill hole data from *Friðleifsson* [1997] and resistivity data from *Sigurðsson* [1965].

South Iceland Seismic Zone (SISZ) in southern Iceland and the Tjörnes Fracture Zone (TFZ) in northern Iceland. Earthquakes in northern Iceland occur mainly along the TFZ. This transform zone links the Northern Volcanic Zone to the Kolbeinsey Ridge, north of Iceland (Figure 1a). Most seismicity within the TFZ occurs along the Grímsey Oblique Rift and the Húsavík-Flatey Fault. The thickness of the crust decreases from 20 km near the

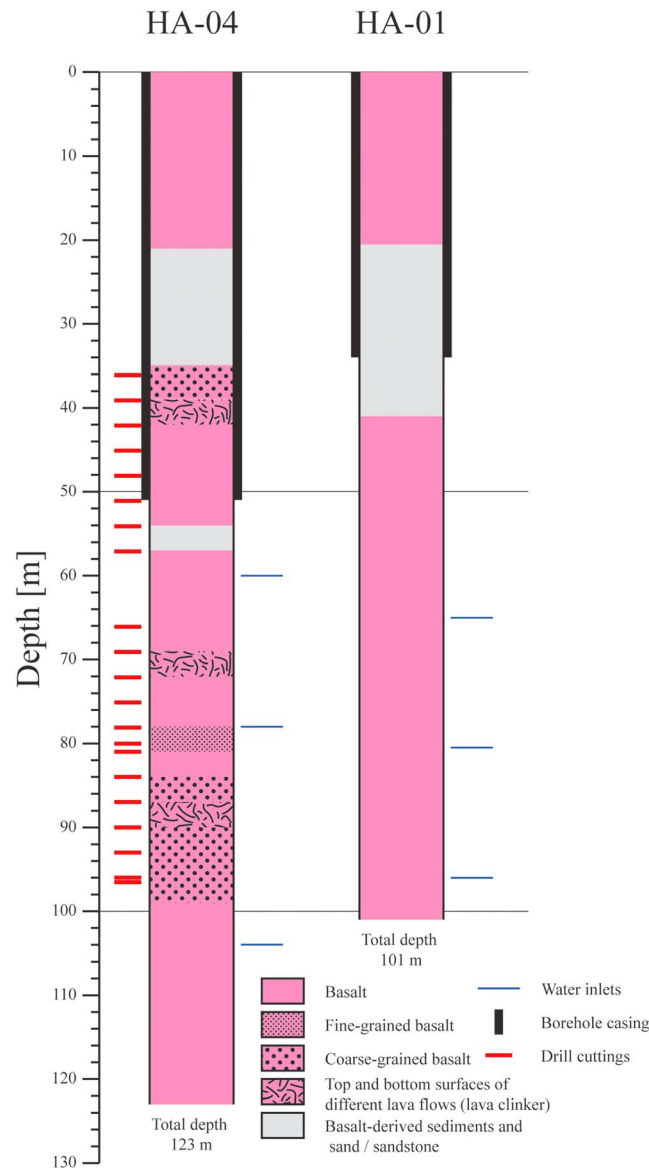


Figure 3. Profiles of the boreholes HA-04 and HA-01. HA-04 penetrates three lava flows beneath the sandstone. There are three water inlets in the boreholes at about 60 m, 80 m, and 100 m. Drill hole HA-01 drilled 1964, data originate from an unpublished drill report by Rafmagnsveitur Ríkisins Jarðborunardeild (1964) and drill hole HA-04 drilled 1996 from Friðleifsson [1997] and unpublished report from drilling company Alvarr ehf. – boranir og verkfræðipjónusta (1996). The red bars mark at which depth the drill cuttings were taken.

Lava, which is about 2000 years old [Sæmundsson, 1991]. Water samples were taken from borehole HA-01 (65.8725°N, 17.4525°W). This borehole is 101 m deep and cased down to 35 m with water inlets at 65 m, 81.5 m, and 95.7 m [Ólafsson, 2011]. It is flowing artesian and as it provides water to the nearby community, Hafralækur the geochemistry has been monitored by the Iceland GeoSurvey (ISOR) periodically since 1974. The ISOR data for the period 1974–2007 are compiled in a report by Ólafsson [2011]; the conclusion of which is that the variations in major ion concentrations, pH, and temperature are minimal during this time period. They reported an average pH of 10.3 (measured at ~18°C) and an average temperature of 73.2°C. Drill cuttings were taken from borehole HA-04 (65.8722°N, 17.4528°W) in 1996 [Friðleifsson, 1997]. This 123 m deep borehole is situated 20 m from HA-01 (Figure 2). The main water inlets in HA-04 are at 60 m, 78–81 m, and 104 m, i.e., at

Húsavík-Flatey Fault to 8 km close to the Grímsey Oblique Rift [Riedel et al., 2005]. The most recent land-based earthquakes in the TFZ were two M 6.5 earthquakes in 1872 destroying all houses in the town of Húsavík [Stefánsson et al., 2008]. Since 1872, all $M > 5$ earthquakes have occurred offshore. The most recent volcanic activity near our study area was the Holuhraun eruption, which began in August 2014 and ended in February 2015 [Sigmundsson et al., 2014].

The boreholes at Hafralækur are situated in a low-temperature geothermal area in the TFZ, 20 km south of Húsavík town (Figure 1b). The water has a low content of dissolved solids (240 ppm), which is typical of low-temperature geothermal waters on the flanks of active rift zones in Iceland [Kristmannsdóttir et al., 2010]. Hydrogen isotope values indicate mixing of modern day (Holocene) meteoric water ($\delta^2\text{H} \sim -70$ ‰ at Hafralækur) and pre-Holocene meteoric water ($\delta^2\text{H} < -106$ ‰) [Árnason, 1977]. Water-rock interaction can be inferred from oxygen isotope values, which are up to 7‰ less negative than the Global Meteoric Water Line [Sveinbjörnsdóttir et al., 2013]. The boreholes penetrate basalts and basalt-derived sediments. Basalts on Iceland contain on average 40–50 % plagioclase of labradoritic composition, 40–50 % pyroxenes of augitic composition, as well as Fe and Ti oxides and sometimes olivine of forsteritic composition [Sæmundsson and Gunnlaugsson, 2014]. Rapidly cooled magma contains basaltic glass, which is enriched in Na and K [Larsson et al., 2002]. However, basaltic glass was not seen in drill cuttings from Hafralækur.

The uppermost layer of the basalt at Hafralækur consists of Younger Laxá

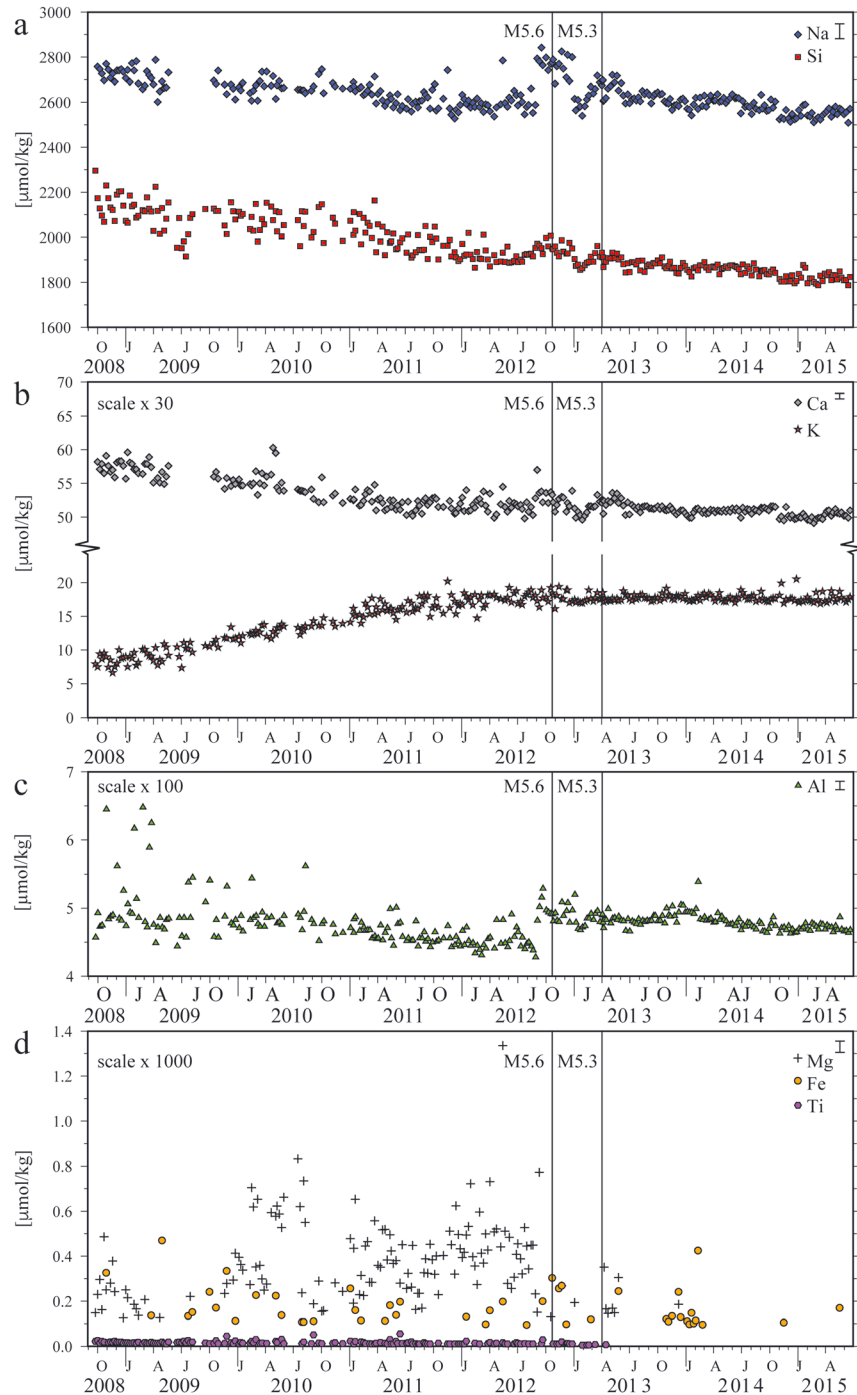


Figure 4. Time series for (a) Na and Si, (b) Ca and K, (c) Al, and (d) Mg, Fe and Ti concentrations in groundwater samples from Hafraalækur collected from September 2008 to June 2015. Data from 30 September 2008 to 4 June 2014 are from Skelton *et al.* [2014] and data from 11 June 2013 to 20 June 2015 are from this study. Data from Skelton *et al.* [2014] were recalculated based on replicate analyses of five samples which were chosen to span the range of concentrations seen during our study. This was necessary because we used a new analytical approach in this study to reduce silicate precipitation (see text for details). This mainly affected Si concentration which Skelton *et al.* [2014] underestimated by a factor of 1.85 ± 0.01 . The corresponding factors for Na, Ca, K, and Al were 0.87 ± 0.01 , 1.27 ± 0.01 , 0.40 ± 0.01 , and 1.01 ± 0.01 . Note that Skelton *et al.* [2014] report concentrations in parts per million, whereas concentrations are reported in $\mu\text{mol/l}$ in the present study. These time series show an overall decrease in the concentrations of Si, Na, and Ca throughout the study with short-lived increases at the times of the $M > 5$ earthquakes. The element K shows an opposite trend with increasing concentrations until the earthquakes followed by a constant concentration. There is no major change in Al concentration throughout our study. The 2σ errors are generally better than 2% as illustrated by error bars in the top right corners. Data for Mg, Fe, and Ti show concentrations that were extremely low, often below detection limits, and with higher uncertainty (10%). The magnitudes shown are of the largest earthquakes to occur on 21 October 2012 ($M 5.6$) and 2 April 2013 ($M 5.3$). The latter has been revised from $M 5.5$ to $M 5.3$ based on updated information from the Global Centroid Moment Tensor Project since publication of the paper by Skelton *et al.* [2014].

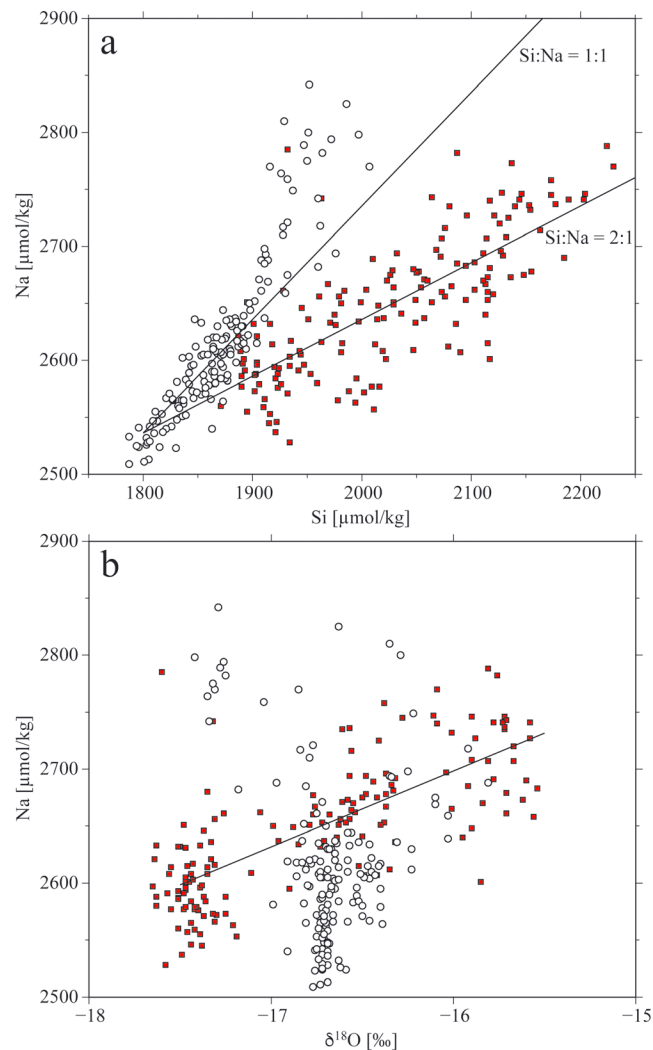


Figure 5. Plot of (a) Na versus Si and (b) Na versus $\delta^{18}\text{O}$ color coded for before and after the abrupt change 2 months before the first earthquake, i.e., October 2008 to August 2012 (filled squares) and September 2012 to June 2015 (open circles).

concentrated nitric acid (1 vol %) for analysis of Na, Ca, Mg, K, Si, Al, Fe, and Ti and the other without acid for analysis of Cl, F, SO_4 , $\delta^2\text{H}$, and $\delta^{18}\text{O}$. All the bottles were stored at $\sim 5^\circ\text{C}$ between collection and analysis. Cations were analyzed using a Thermo inductively coupled Argon plasma 6500 Duo optical emission spectrometer (ICP-OES), and anions were analyzed using a Dionex DX-300 ion chromatography system at Stockholm University. These analyses and methods are described in detail in Skelton *et al.* [2014]. From June 2013 onward, cations and anions were instead analyzed at the University of Iceland, Reykjavik, Iceland, using a Spectro Ciros Vision inductively coupled plasma optical emission spectrometer (ICP-OES). Replicates between Stockholm University and University of Iceland, which were chosen to span the range of concentrations seen during the study showed systematic shifts for Si ($\times 1.85 \pm 0.01$), Na ($\times 0.87 \pm 0.01$), Ca ($\times 1.27 \pm 0.01$), K ($\times 0.40 \pm 0.01$), and Al ($\times 1.01 \pm 0.01$). Analyses of geothermal water containing high amounts of Si and Na are known to induce Na-silicate precipitation on the glass nebulizers used in ICP-OES analysis. This may lead to larger errors and/or blockage of the nebulizer. For the analyses in Iceland, silicate precipitation was kept to a minimum by a combination of short analytical runs and daily cleaning of the nebulizers with aqua regia using a sonicator between runs. To further minimize the analytical problems caused by silicate precipitation, a new Mira Mist Teflon nebulizer from Burgener Research Inc. was used for analysis of the samples from November 2014 and onward. The analyses performed in Iceland are considered more reliable and are reported in this study.

similar depths as HA-01 (Figure 3), and the pH and water temperature at HA-04 were measured to 10.2 (at 20°C) and $60\text{--}70^\circ\text{C}$, respectively, i.e., a slightly lower temperature than for HA-01 [Friðleifsson, 1997]. Borehole HA-04 penetrates a layer of basalt-derived sediments beneath the Younger Laxá Lava and thereafter three lava flows (Figures 2 and 3).

3. Methods

From September 2008 to June 2015 water samples were collected on a weekly basis from borehole HA-01. As it is flowing artesian, water was sampled directly from the surface. The pH was monitored from June 2013 onward. For logistical reasons, such as weather conditions, samples were taken to an indoor facility, where pH was measured at room temperature ($\sim 20^\circ\text{C}$) on the same day that the samples were taken using a Hanna Instruments portable pH meter HI-8424. The alkalinity was determined later by HCl titration using a Radiometer Analytical TitrLab Titration Workstation at Stockholm University, Sweden. Also, additional samples were analyzed for total dissolved carbonate within 2 days of sample collection at the Efla Engineering firm in Reykjavik, Iceland, by automatic HCl equilibrium titration using a Metrohm Titrino 794.

The water samples were filtered in situ by syringing the water through a $0.2\ \mu\text{m}$ filter into two separate acid-washed $125\ \text{cm}^3$ LDPE bottles, one together with

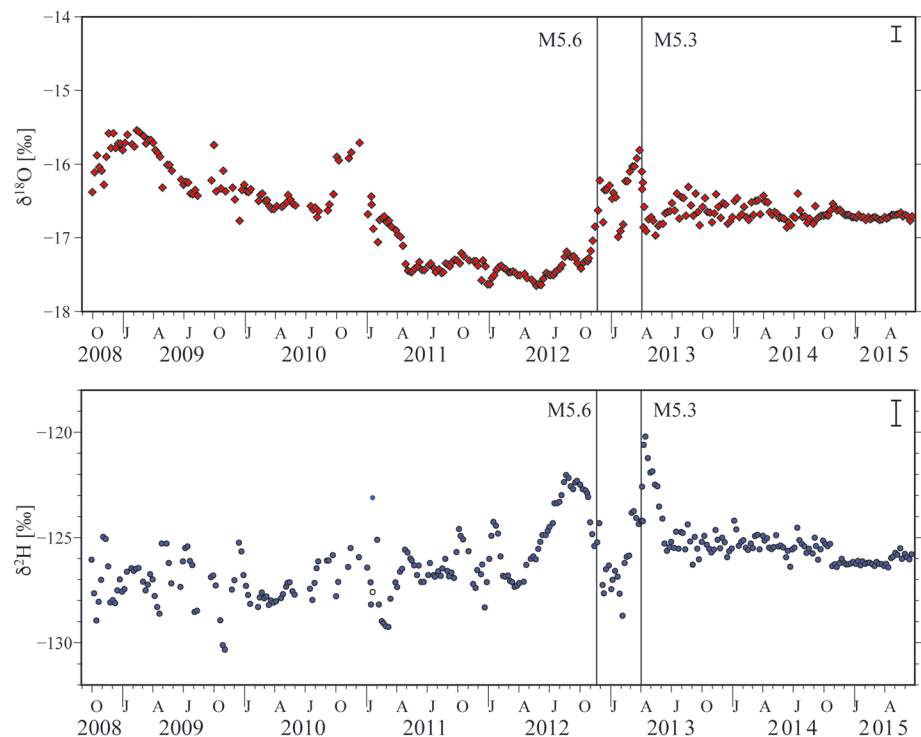


Figure 6. Time series for oxygen ($\delta^{18}\text{O}$) and hydrogen ($\delta^2\text{H}$) isotopic values from 2008 to 2015. Changes correlate with both $M > 5$ earthquakes. Error bars are shown in the top right corners.

The accuracy of these measurements was monitored using in-house standards calibrated against commercial certified standards. For most major elements, the error at 95% confidence level was always below 3%.

Oxygen ($\delta^{18}\text{O}$) and hydrogen ($\delta^2\text{H}$) isotopic values were measured using a cavity ring down spectroscopy instrument from Los Gatos Research (Liquid Water Isotope Analyzer model). Both $\delta^{18}\text{O}$ and $\delta^2\text{H}$ were normalized so that the difference between Vienna Standard Mean Ocean Water (VSMOW) and standard light Antarctic precipitation was -55.5‰ for $\delta^{18}\text{O}$ and -428‰ for $\delta^2\text{H}$. The error in analysis of the measurements was better than $\pm 0.6\text{‰}$ for the $\delta^2\text{H}$ values and $\pm 0.1\text{‰}$ for the $\delta^{18}\text{O}$ values.

Twenty drill cutting samples from borehole HA-04, evenly spaced (where possible) between depths of 36 and 96 m, were provided by the Iceland GeoSurvey (ISOR) in Reykjavik, Iceland. The drill cuttings were examined using a binocular microscope, and the largest grains (which are 5–15 mm in size) were handpicked, mounted in epoxy, and made into thin sections. Thin sections were used for mineral identification, estimation of mineral modes, textural studies, and for determination of mineral chemistry by electron probe microanalysis (EPMA). Point analyses, profiles, and chemical maps were made using a JEOL JXA-8530 F field emission gun electron probe microanalyser (FEG-EPMA) at the Department of Earth Sciences, Uppsala University, Sweden, following the procedure outlined in *Weis et al.* [2015] using the following standards: fayalite for Fe, MgO for Mg, pyrophanite for Mn and Ti, Al_2O_3 for Al, wollastonite for Ca and Si, albite for Na, and orthoclase for K. FEG-EPMA operating conditions were 15 kV and 20 nA. We used variable spot sizes ranging from 1 μm for primary minerals to 10 μm for some secondary minerals. The reason for using a large spot size was to avoid preferential loss of lighter elements such as Na.

After removal of the largest grains and homogenization of the remaining sample by mixing, a part (typically 1 g) was powdered, and aliquots were used for determination of major element concentrations by X-ray fluorescence spectrometer, stable isotope ($\delta^{18}\text{O}$) analysis by mass spectrometry, mineral identification, and quantification by X-ray diffraction (XRD).

Major element compositions were determined using an X-ray fluorescence spectrometer at the School of GeoSciences, University of Edinburgh, Scotland. Samples were fused with a lithium metaborate-lithium carbonate flux containing La_2O_3 as a heavy absorber (Johnson Matthey Spectroflux 105), using a method similar to that developed by *Norrish and Hutton* [1969]. Sample powder was dried at 110°C overnight, and

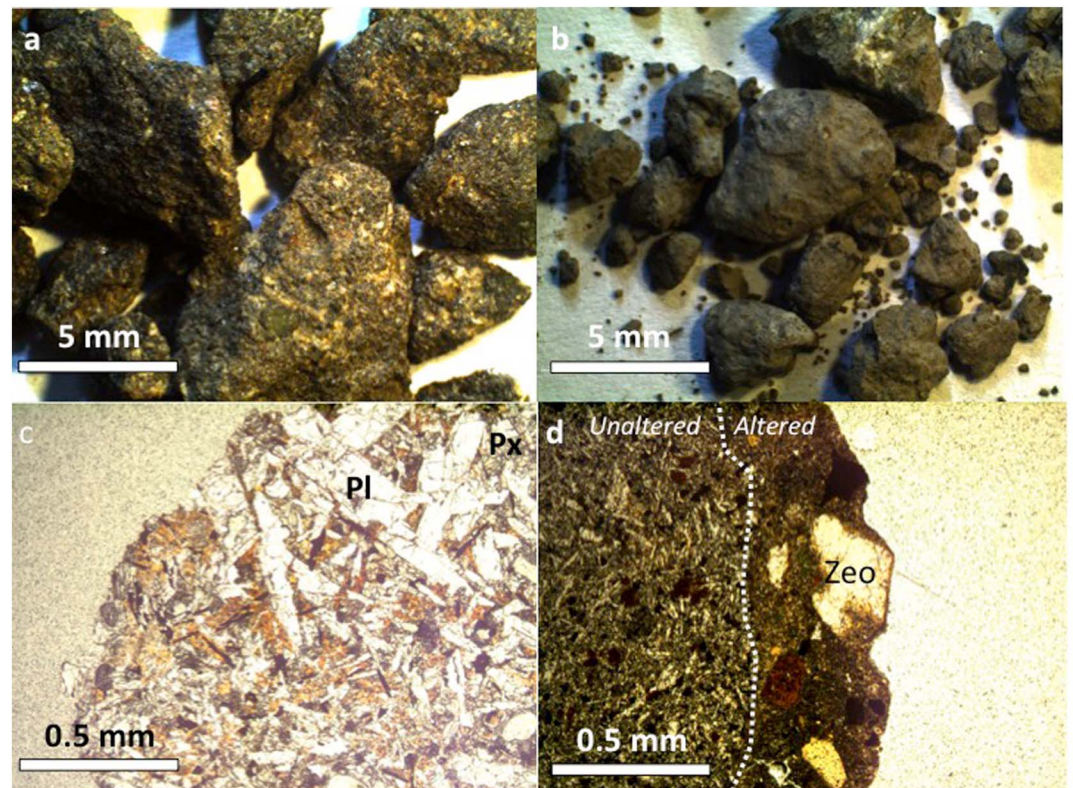


Figure 7. Photomicrographs of drill cuttings from borehole HA-04 showing (a) comparatively fresh subangular dark colored grains from a depth of 87 m, i.e., far from a water inlet and (b) comparatively altered subrounded pale coloured grains from a depth of 80 m, i.e., close to a water inlet. The figure also shows thin sections of (c) fresh grains containing plagioclase (Pl) and pyroxene (Px) at a depth of 87 m and (d) grains with fine-grained altered rims containing zeolites (Zeo) at a depth of 80 m.

a nominal but precisely weighed 1 g aliquot was ignited at 1100°C to determine loss on ignition (LOI). The residue was then mixed with flux in a sample flux ratio of 1:5 based on the unignited sample weight. The mixture was then fused at 1100°C in Pt5%Au crucibles in a muffle furnace. After initial fusion, the crucible was reweighed, and any weight loss from the flux was made up with additional flux to maintain the 1:5 sample flux ratio as closely as possible. After a second fusion and homogenisation over a Meker burner the molten sample flux mixture was cast onto a graphite mold and flattened with an aluminum plunger. During this process, the mold and plunger were kept at 220°C on a hot plate.

The fused discs were analyzed on a Philips PW2404 X-ray fluorescence spectrometer with a Rh-anode primary X-ray tube. Corrections for matrix effects on the intensities of the major element fluorescence lines were made using theoretical alpha coefficients calculated using Philips software. The coefficients were calculated to allow for the amount of extra flux replacing volatile components in the sample lost during the LOI step, so that analytical totals should be 100% less the LOI. The spectrometer was calibrated using a suite of ten USGS and CRPG standards the values of which are given in Govindaraju [1994]. Calibration lines show that accuracy and precision are closely similar with an average 1σ value across the 10 elements of 0.03 wt %.

Mineral identification and quantitative phase analysis by XRD was done at the Natural History Museum, University of Copenhagen, Denmark. The instrument used was a Bruker-AXS Advance 8 powder diffractometer in a Bragg-Brentano (reflection) geometry, equipped with a Cu tube, Ge111 primary beam monochromator (wavelength $K_{\alpha 1} = 1.540596 \text{ \AA}$), and the Silicon-strip LynxEye detector (range 3.3°). Fixed slit (divergence angle 0.45°) was used, and the samples were measured in 5 to 90° 2θ range (highest resolution 1.09 \AA). After identification of minerals with the help of probability density function and inorganic crystal structure databases, the accurate unit cell parameters and proportion of minerals were determined by the Rietveld method [Rietveld, 1969] using the computer program Topas 4.2 (from Bruker-AXS). Fundamental parameters approach was used, and the instrument profile parameters were refined on CeO_2 standard with known average crystallite size.

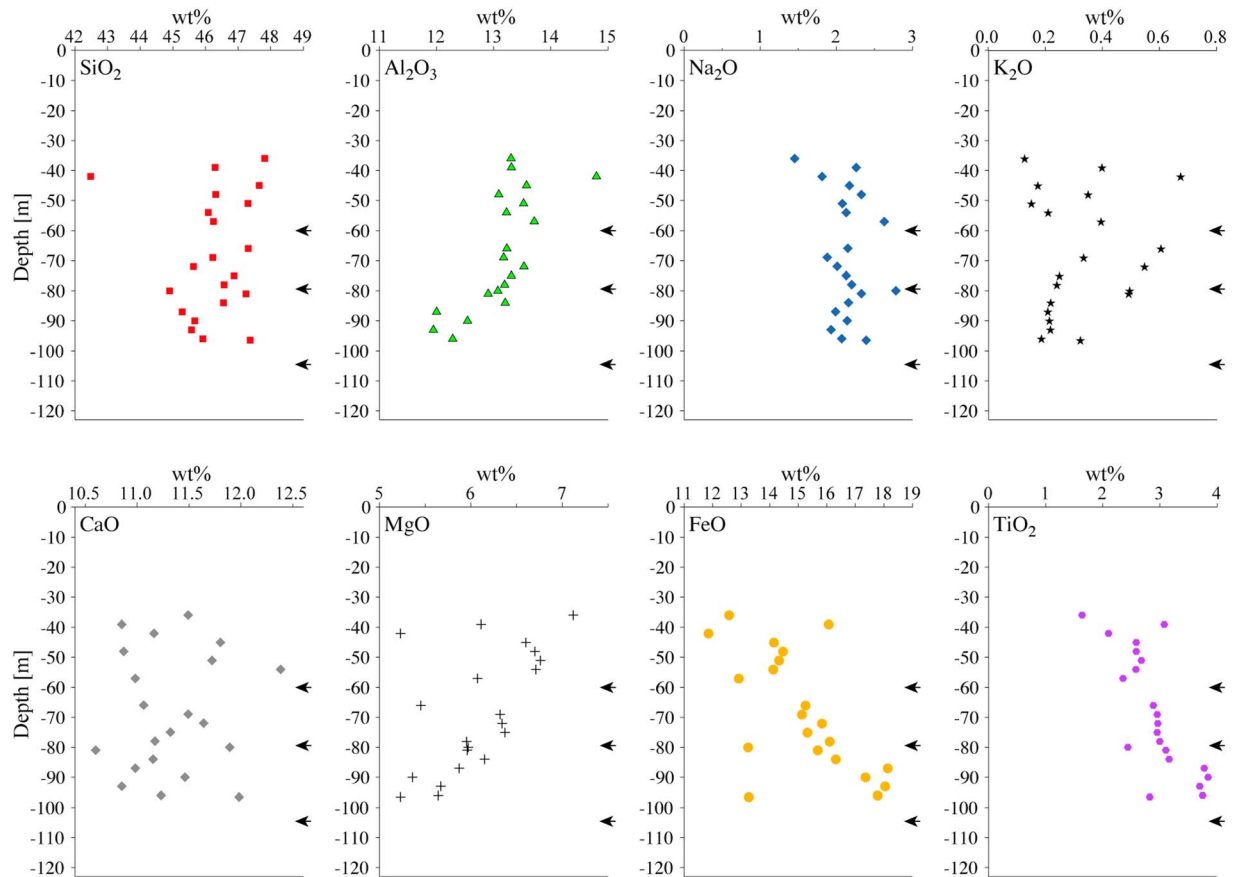


Figure 8. Concentrations of SiO₂, Al₂O₃, Na₂O, K₂O, CaO, MgO, and FeO in drill cuttings taken from the 123 m deep borehole HA-04. Water inlets at 60, 80, and 104 m are marked with black arrows. The 2σ error is better than 0.1% for major elements (error bars are too small to be visible).

Mineral identification by Raman spectroscopy was done from thin sections and on rock chips from the drill cuttings at the Department of Geological Sciences, Stockholm University, Sweden. The instrument used was an Horiba instrument LabRAM HR 800 (Horiba Jobin Yvon) confocal laser Raman spectrometer equipped with a multichannel air-cooled (−70°C) 1024 × 256 pixel charge-coupled device detector. Excitation was provided by an Ar-ion laser (λ = 514 nm) source. Spectra were recorded using a laser power of 5 mW at the sample surface. An Olympus BX41 microscope was coupled to the instrument. The laser beam was focused through an 80x objective with a working distance of 8 mm to obtain a spot size of about 1 μm. The accuracy of the instrument was controlled by repeated use of a silicon wafer calibration standard with a characteristic Raman line at 520.7 cm^{−1}.

Linking between changes of groundwater chemistry and evidence of mineral reactions was aided by using the geochemical modeling program Phreeqc Interactive version 3.1.7 [Parkhurst and Appelo, 1999] together with its database lnl.dat, which contains most of the primary and secondary minerals found in the drill cuttings, e.g., zeolites. The program provides information about element speciation in water and saturation indices of minerals, i.e., which minerals should dissolve and which minerals could precipitate based on thermodynamic calculations. In addition, the program can recalculate conditions at a different temperature than that at which a water sample was analyzed, i.e., field temperature.

4. Results

4.1. Groundwater Chemistry

The pH of groundwater from HA-01 was 10.10 ± 0.04 measured at 20.7 ± 0.5°C from 2013 to 2015. The in situ temperature of water sampled from borehole HA-01 was measured to 68°C in June 2015, which is 5° lower

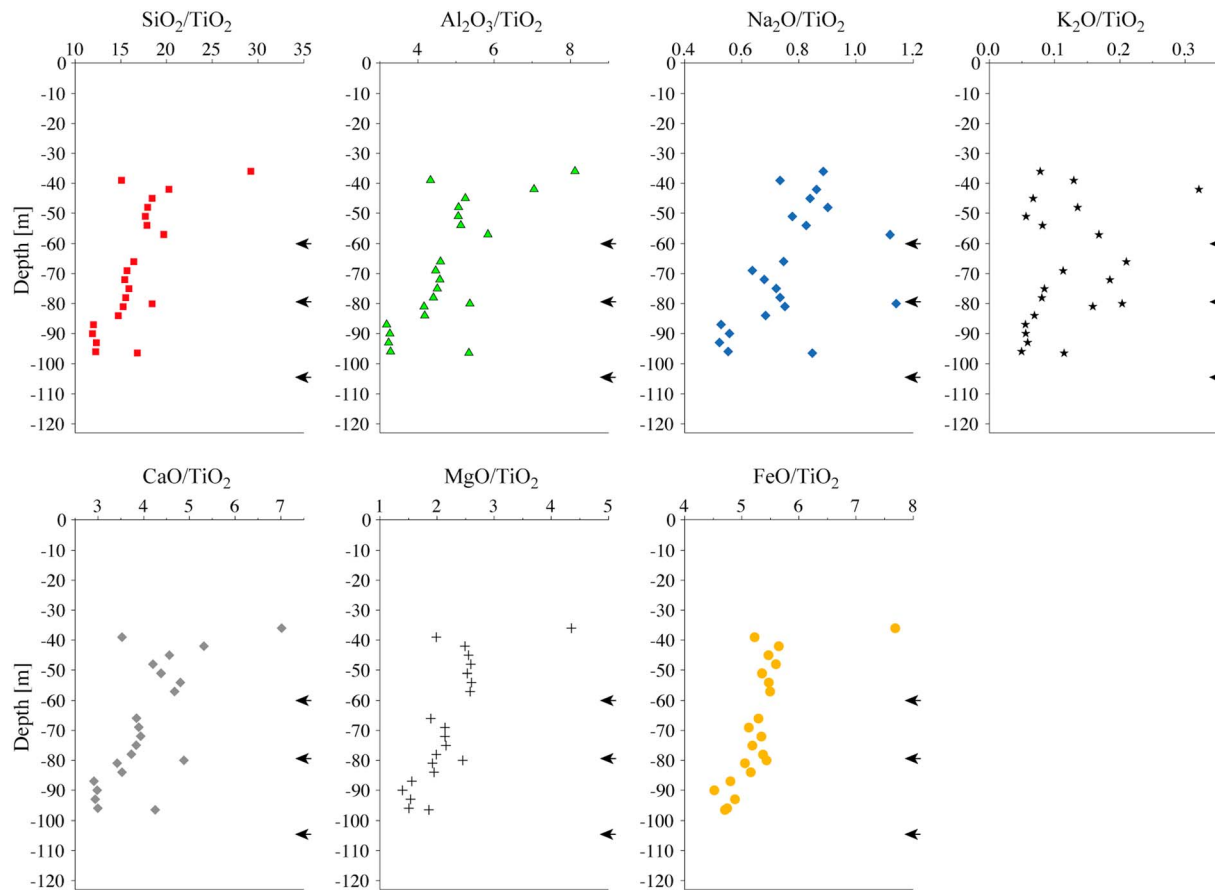


Figure 9. TiO₂-normalized concentrations of SiO₂, Al₂O₃, Na₂O, K₂O, CaO, MgO, and FeO in drill cuttings taken from the 123 m deep borehole HA-04. Water inlets at 60, 80, and 104 m are marked with black arrows. The 2σ error is better than 0.1% for major elements (error bars are too small to be visible).

than the average temperature measured by ISOR for the period 1974–2007 [Ólafsson, 2011]. There was a gradual decrease in alkalinity throughout the study from 2.2 to 1.8 meq/kg. At this high pH, the alkalinity depends mainly on the silicate equilibrium system where H₄SiO₄⁰ dissociates to H₃SiO₄⁻ in low-temperature geothermal waters [Stefánsson *et al.*, 2001]. Hence, alkalinity is mainly due to H₃SiO₄⁻ anions, whereas the carbonate contribution is smaller: on average ~310 μmol/kg total C (ranging from 114 to 640 μmol/kg). The concentrations of other anions are ~280 μmol/kg Cl, ~50 μmol/kg F, and ~250 μmol/kg SO₄. Time series were constructed from September 2008 to June 2015 for the concentrations of the elements, which are major constituents of the basaltic host rock (Si, Al, Na, K, Ca, Mg, Fe, and Ti). Time series for Si, Al, Na, K, Ca, Mg, Fe, and Ti are shown in Figure 4. Concentrations of Mg, Fe, and Ti in groundwater were close to or below detection limits (3–5 ppb) for most of the study period. Ti was not part of the ICP-OES analysis performed at the University of Iceland; hence, no Ti data exist from June 2013 onward. All water analysis results from HA-01 are provided in the supporting information.

The data for Si, Na, Ca, and K for the period September 2008 to June 2013 were previously published by Skelton *et al.* [2014]. These authors reported a slow decrease in Si and Na concentrations, an order-of-magnitude smaller decrease of Ca concentration, and concomitant increase of K concentration from September 2008 to August 2012. They also reported a statistically significant increase of Na concentration before each *M* > 5 earthquake. The first concentration increase was abrupt and occurred between 28 August and 3 September 2012, *i.e.*, 2 months before the first earthquake (Figure 4). In this study, we have extended the time series published by Skelton *et al.* [2014] for these elements to June 2015. These data are shown together with the other cations that are abundant in the basaltic host rock, *i.e.*, Al, Mg, Fe, and Ti. These extended time series allow us to compare groundwater chemistry before and after this abrupt change of chemical behavior, 2 months before the first earthquake (Figures 4 and 5):

Table 1. Volume Percent of Minerals in Drill Cuttings of HA-04^a

Depth(m)	Plagioclase	Augite	Ilmenite	Magnetite	Hematite	Smectite	Analcime	Chabazite	Stilbite	Epistilbite	Thomsonite	Natrolite	Gobbsinite	Samidine	Calcite
36	34.9(4)	32.6(4)	0.5(1)	0.8(2)	0.5(1)	14.9(5)	--	7.5(2)	8.3(2)	--	--	--	--	--	--
39	52.8(4)	32.9(3)	2.6(2)	1.5(1)	1.5(1)	4.2(4)	--	2.3(1)	--	2.0(1)	--	--	--	--	--
42	5.5(2)	22.7(4)	0.28(9)	0.7(2)	6.5(2)	4.8(9)	7.8(2)	21.7(3)	--	3.4(2)	21.4(4)	1.1(2)	--	4.2(3)	--
45	51.8(4)	35.5(4)	1.7(1)	2.2(2)	0.13(7)	8.8(5)	--	--	--	--	--	--	--	--	--
48	33.1(4)	31.6(5)	2.0(1)	1.8(2)	0.4(1)	10.4(8)	4.1(1)	6.9(2)	--	--	5.7(2)	--	4.1(2)	--	--
51	52.6(4)	35.5(3)	2.1(1)	1.1(1)	0.08(6)	8.6(5)	--	--	--	--	--	--	--	--	--
54	52.7(4)	35.3(4)	2.0(2)	1.8(3)	0.5(2)	6.7(5)	1.1(1)	--	--	--	--	--	--	--	--
57	31.9(3)	29.7(4)	1.5(1)	0.5(1)	0.4(1)	9.7(6)	12.6(2)	3.6(1)	--	--	8.4(3)	--	1.8(2)	--	--
66	48.1(4)	31.7(4)	2.0(2)	1.3(2)	1.0(1)	11.4(5)	--	2.0(1)	2.5(2)	--	--	--	--	--	--
69	46.4(4)	36.3(4)	1.5(1)	2.9(2)	0.3(1)	7.4(5)	--	2.2(2)	2.1(2)	1.0(2)	--	--	--	--	--
72	52.5(4)	35.6(4)	1.7(2)	2.0(2)	1.2(2)	5.6(5)	--	0.6(1)	--	0.8(2)	--	--	--	--	--
75	52.3(4)	34.2(4)	2.3(1)	1.5(2)	0.11(7)	6.6(5)	--	1.1(2)	1.9(2)	--	--	--	--	--	--
78	50.4(4)	33.8(4)	2.0(1)	2.4(2)	0.13(7)	9.2(5)	--	--	2.1(2)	--	--	--	--	--	--
80	36.9(4)	35.6(4)	2.6(2)	1.3(2)	--	2.2(4)	8.0(1)	2.7(1)	--	--	5.8(3)	--	3.1(4)	--	1.9(1)
81	56.9(4)	31.7(4)	2.6(2)	2.7(2)	0.09(7)	6.0(6)	--	--	--	--	--	--	--	--	--
84	53.7(4)	34.8(4)	3.3(2)	1.1(2)	0.32(8)	6.8(5)	--	--	--	--	--	--	--	--	--
87	51.5(5)	35.5(5)	2.6(2)	1.0(2)	0.3(1)	9.0(7)	--	--	--	--	--	--	--	--	--
90	51.5(5)	34.8(5)	2.4(2)	1.2(2)	0.3(2)	8.7(6)	--	--	--	0.9(3)	--	--	--	--	--
93	46.0(5)	34.3(5)	2.9(2)	1.1(2)	1.1(2)	14.1(8)	--	--	--	0.4(2)	--	--	--	--	--
96	52.9(5)	33.5(4)	2.4(2)	2.2(2)	0.23(7)	7.7(6)	--	--	--	1.0(2)	--	--	--	--	--

^aModal estimates for drill cutting samples made by X-ray diffraction. The numbers in parentheses are estimated standard deviations referred to the last significant digit and as determined by the Rietveld least squares refinement (program Topas 4.2 from Bruker-AXS). The expected realistic errors of analysis are 2 to 3 times larger than the standard deviation determined by the method.

1. Before this change occurred, Si and Na concentrations decreased gradually with a ratio of 2:1 (Figure 5). There was also a concomitant *but order-of-magnitude smaller* decrease of Ca concentration and increase of K concentration. There was no appreciable change of Al concentration.
2. The abrupt change occurred between 28 August and 3 September 2012. Na concentration increased dramatically. There were smaller increases of Si and Ca concentration, but these are not separable from normal variation. There was a slight change of Al concentration, but this was less than the analytical error. K concentration was unchanged.
3. Na peaks coincided with both earthquakes. Thereafter, Si and Na concentrations decreased with an initial ratio below 1:1, which gradually returned toward 2:1 after the second earthquake (Figures 4 and 5). There were no significant changes of Ca, K, or Al concentrations.
4. The concentrations of Fe, Mg, and Ti were close to detection limits throughout the study. No systematic variation was observed (Figure 4).

From September 2008 to June 2015 groundwater oxygen ($\delta^{18}\text{O}$) isotopic values varied between -17.6‰ and -15.5‰ and the hydrogen ($\delta^2\text{H}$) values from -130 to -120‰ (Figure 6). Both isotopes showed changes associated with earthquakes. Abrupt changes of $\delta^{18}\text{O}$ values coincide with both earthquakes, and the coincidence of $\delta^2\text{H}$ anomalies with both earthquakes first reported by Skelton *et al.* [2014] is confirmed by the extended time series. Using the same binomial test as Skelton *et al.* [2014], we obtain a revised p value of $10^{-5.5}$ for probable association of the $\delta^2\text{H}$ and Na maxima with both earthquakes. This compares with the p value of 10^{-5}

Table 2. Representative EPMA Analyses^a

Mineral	Depth	Measured Weight Percent Oxides										Chemical Formula (a.p.f.u.)							
		Na ₂ O	SiO ₂	Al ₂ O ₃	MgO	MnO	TiO ₂	K ₂ O	CaO	FeO	Total	Na	Si	Al	Mg	Ca	Fe	O	
Pyroxene	82 m	0.25	51.35	2.18	14.98	0.38	1.07	0.02	19.12	10.23	99.58	0.02	2.42	0.12	0.53	0.97	0.40	6.00	
Plagioclase ¹	82 m	4.30	52.59	28.63	0.17	0.03	0.16	0.18	12.67	1.08	99.81	0.38	2.43	1.55		0.63		8.00	
Plagioclase ²	42 m	3.44	51.83	28.97	0.23	0.03	0.06	0.10	13.34	0.75	98.75	0.31	2.41	1.58		0.66		8.00	
Plagioclase ³	42 m	4.75	55.49	29.54	0.25	0.04	0.16	0.13	11.80	0.71	102.87	0.41	2.46	1.54		0.56		8.00	
				<i>Labradorite</i>									0.40	2.40	1.60		0.60		8.00
Zeolite ¹	42 m	11.07	56.25	23.32	0.04	0.10	0.07	0.02	0.21	0.05	91.27	0.78	2.05	1.00		0.01		6.00	
Zeolite ²	42 m	4.77	58.40	24.00	0.02	0.00	0.04	0.18	2.08	0.08	89.57	0.33	2.11	1.02		0.08		6.00	
				<i>Analcime</i>									1.00	2.00	1.00		0.00		6.00
Zeolite ³	42 m	5.41	58.51	24.66	0.08	0.00	0.12	0.26	8.43	2.42	99.90	1.44	8.03	3.98		1.24		24.00	
				<i>Chabazite</i>									1.52	8.00	4.00		1.24		24.00

^aEPMA analyses of representative pyroxene, plagioclase, and zeolites. The compositions of labradorite, analcime, and chabazite are shown for comparison in italics. Pyroxene and plagioclase¹ were from a relatively fresh basalt at a depth of 82 m. The high Si content of pyroxene could reflect partial replacement by smectite. The plagioclase is labradoritic in composition. Plagioclase² is an analysis of the interior of a labradorite crystal from a clast in a breccia at a depth of 42 m. Plagioclase³ is an analysis of the edge of the same labradorite crystal adjacent to analcime. Note that Na and Si concentrations are higher, whereas Ca and Al are lower than in the interior of this crystal. The high total is probably an analytical artifact and might reflect porosity at the edge of the crystal. Zeolite¹ is an analysis of the interior of the adjacent analcime crystal (marked by a cross symbol on Figure 11). Note that Al and Si in atoms per formula unit (a.p.f.u.) are as expected for analcime, but Na in a.p.f.u. is lower than expected. Zeolite² is an analysis of the edge of the same analcime crystal adjacent to labradorite. Note that Na in a.p.f.u. is lower than in the interior of this crystal.

reported by Skelton *et al.* [2014]. Also, based on our extended time series, we obtain *p* values, which are better than 0.1 for probable association based on coincidence of only one anomaly with only one of the earthquakes. For this value to fall below 0.05 requires 10 years of measurements, i.e., our 8 year time series needs to be extended by two more years.

4.2. Drill Cuttings

4.2.1. Macroscopic Observations

Drill cuttings from borehole HA-04 consist of rock fragments, 2–15 mm in size, black to greenish grey in color; some of which contain optically discernible whitish zeolites. These are most abundant in drill cuttings closest to the water inlets at 60 m, 78–81 m, and 104 m. Figure 7 shows representative drill cuttings far from and close to the water inlets. The drill cuttings far from the water inlets (depth = 87 m) are comparatively fresh dark colored subangular grains, 5–10 mm in diameter and composed of primary plagioclase and pyroxene. The drill cuttings close to the water inlets (depth = 80 m) are comparatively altered pale colored subrounded grains, 2–5 mm in diameter, and with highly altered rims containing zeolites.

4.2.2. Whole Rock Chemistry

The concentrations of SiO₂, Al₂O₃, Na₂O, K₂O, CaO, MgO, FeO, and TiO₂ in drill cuttings are plotted against depth in Figure 8 and included as supporting information. This figure shows that the concentrations of SiO₂, Al₂O₃, Na₂O, K₂O, CaO, and MgO decrease, and the concentrations of FeO and TiO₂ increase with depth. Oxide concentrations were normalized to TiO₂ so as to distinguish between chemical variations of magmatic origin and chemical variations caused by water-rock interaction. These data are plotted in Figure 9. This is a first-order approximation, which assumes that the mobility of Ti in groundwater is negligible [Pearce and Norry, 1979]. This assumption is supported by groundwater chemical data at Hafraflækur, which shows that

Table 3. Chemical Formulae of Feldspars and Zeolites Found at Hafraflækur

Group	Mineral	Formula
Feldspar	Labradorite	Na _{0.4} Ca _{0.6} Al _{1.6} Si _{2.4} O ₈
	Sanidine	KAlSi ₃ O ₈
Zeolites	Analcime	NaAlSi ₂ O ₆ H ₂ O
	Chabazite	Ca ₂ Al ₄ Si ₈ O ₂₄ (H ₂ O) ₁₃
	Thomsonite	Na ₄ Ca ₈ Al ₂₀ Si ₂₀ O ₈₀ (H ₂ O) ₂₄
	Stilbite	NaCa ₄ Al ₉ Si ₂₇ O ₇₂ (H ₂ O) ₃₀
	Epistilbite	CaAl ₂ Si ₆ O ₁₆ (H ₂ O) ₅
	Gobbsinite	(Na ₂ ,Ca) ₂ K ₂ Al ₆ Si ₁₀ O ₃₂ (H ₂ O) ₁₂
	Natrolite	Na ₂ Al ₂ Si ₃ O ₁₀ (H ₂ O) ₂

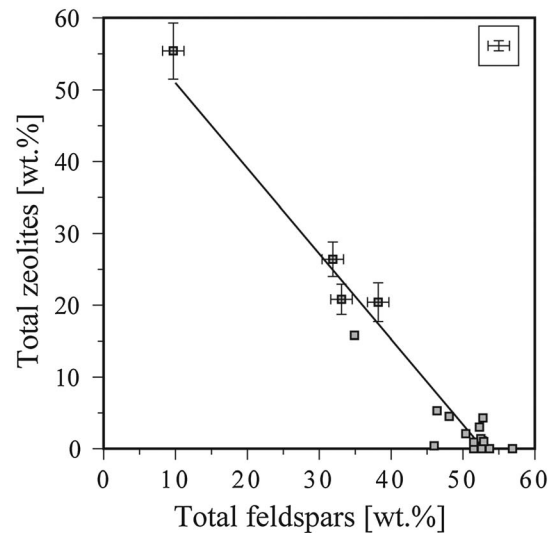


Figure 10. Inverse correlation ($R^2 = 0.95$) between modal feldspars and modal zeolites in drill cuttings from borehole HA-04. The data used to construct this figure are from Table 1. The samples from the breccia (42 m) and the water inlets have higher uncertainty on total zeolites weight percent and are therefore given individual error bars. The remaining samples are represented by the error bars in the top right corner.

The Fe content of augite increases with depth. Minor amounts of ilmenite, magnetite, and hematite were also found. However, neither olivine nor basaltic glass was found (presumably because glass is rapidly replaced by zeolites). The sample at a depth of 42 m is a breccia. This sample contains sanidine in addition to the other primary minerals (Table 1).

The most abundant secondary minerals (identified petrographically, by XRD and by Raman spectroscopy) are smectite, analcime, chabazite, stilbite, and thomsonite (Tables 1 and 3). Calcite was observed in thin section from 80 m depth making microcrystalline rims around pyroxenes. Occurrences of chabazite and thomsonite in vesicles were also

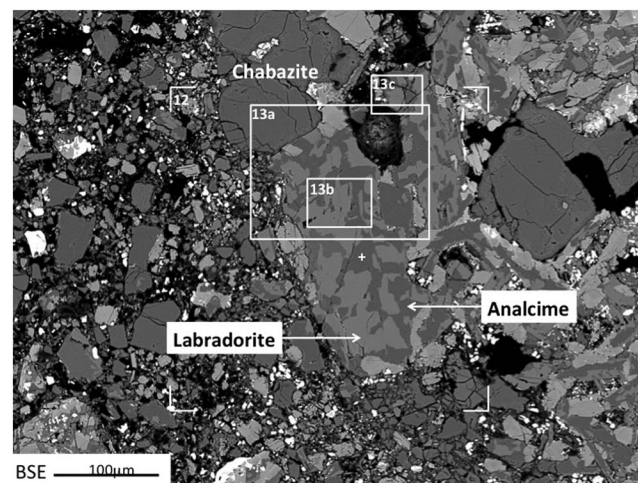


Figure 11. Backscattered electron (BSE) image of breccia from a depth of 42 m in borehole HA-04. Some clasts contain labradorite, which is partly replaced by analcime. Other clasts contain chabazite. The locations of Figures 12 and 13a–13c are shown. The point where analcime was analyzed (Zeolite¹ in Table 2) is marked by a cross symbol. This image was obtained by EPMA at 15 kV.

Ti concentrations are low ($<0.02 \mu\text{mol/kg}$; supporting information). TiO_2 -normalized data show a stepwise depth variation in the concentrations of most elements (Figure 9). These “steps” correlate approximately with water inlets. No steps were seen in the $\text{K}_2\text{O}/\text{TiO}_2$ data, which show considerable scatter. In addition to steps, TiO_2 -normalized concentrations of Si, Na, and Ca peak close to each of the water inlets. This is most clearly seen for the $\text{Na}_2\text{O}/\text{TiO}_2$ data. Using a Shapiro Wilk test, we were able to confirm that the $\text{Na}_2\text{O}/\text{TiO}_2$ peaks at 57 m and 80 m (i.e., close to the upper 2 water inlets) are genuine anomalies and not simply part of a normal distribution about the stepped depth profiles (p value = 0.002). It is also likely that the peak at 96 m (i.e., close to the lower water inlet) is not part of this normal distribution (p value = 0.07). However, we cannot eliminate this null hypothesis for the corresponding $\text{SiO}_2/\text{TiO}_2$ and CaO/TiO_2 peaks.

4.2.3. Mineralogy

The primary minerals in drill cuttings from borehole HA-04 (identified petrographically, by XRD and by EPMA) are labradorite and augite (Tables 1 and 2).

recorded in the drilling report published by the Icelandic Energy Authority [Fridleifsson, 1997]. The proportions of plagioclase and zeolites correlate inversely (Figure 10).

In thin section, chabazite was seen to fill vesicles, and analcime was seen to partially replace labradorite. This is seen on backscattered electron (BSE) images (Figure 11) and on element maps for Na and Ca (Figure 12). Color enhancement of the BSE image reveals atomic density peaks at the edges of labradorite crystals alongside analcime or fractures and at the edges of chabazite crystals alongside fractures (Figure 13). Chemical profiles across an interface between labradorite and analcime and across a fracture along such an interface (Figure 14) reveal $\sim 5 \mu\text{m}$ wide boundary layers across which SiO_2 concentration

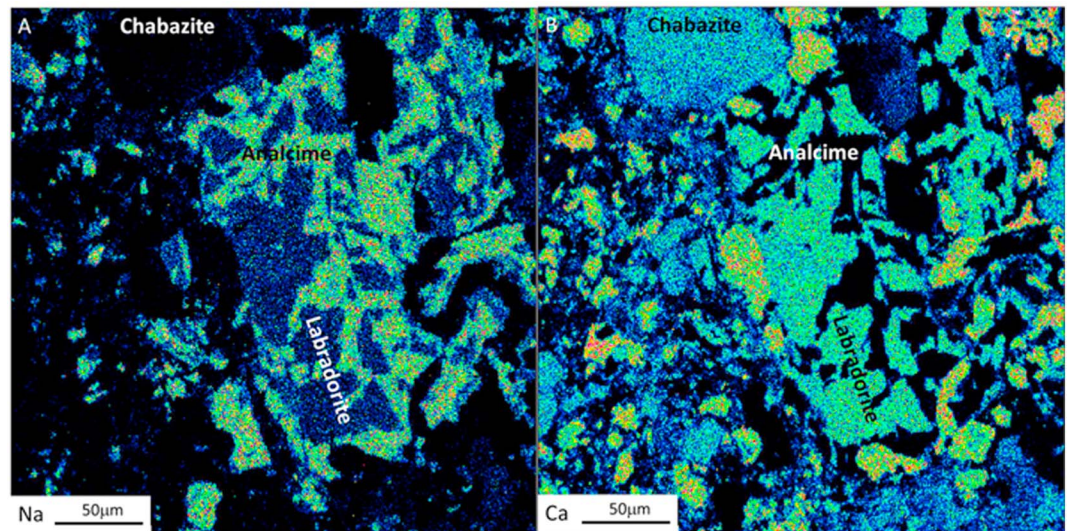


Figure 12. Element maps for Na and Ca of the area shown in the BSE image in Figure 11. Patchy replacement of labradorite by more sodic but less calcic analcime is seen. Chabazite is more calcic and less sodic than analcime. These images were obtained by EPMA at 15 kV. The color scale is from low (blue and green) to high (yellow and red) element concentration.

increases gradually from ~52 wt % in labradorite to >60 wt % in analcime, CaO concentration decreases from 12–14 wt % in labradorite to ~0 wt % in analcime, and Al_2O_3 concentration decreases from 28–30 wt % in labradorite to 22–24 wt % in analcime. The concentration of Na_2O increases from ~3.5 wt % in labradorite, peaking at ~5 wt % at the midpoint of the unfractured boundary layer. The concentration of Na_2O in analcime decreases toward the fracture. The concentration of Na_2O in analcime outside these boundary layers was much higher (11 wt % compared with 4–7 wt %) but nevertheless lower than for stoichiometric analcime (14.09 wt %). The peak in Na_2O concentration at the midpoint of the boundary layer coincides spatially with a peak in atomic density seen on the BSE images. Comparison of a sequence of Raman spectra taken across this boundary layer with reference spectra from the RRUFF database (<http://rruff.info/>) [Downs, 2006] reveals a transition from labradorite to analcime within this layer (Figure 15). This transition corresponds with the gradient in SiO_2 data seen across this layer (Figure 14). The most prominent Raman bands can be assigned to vibration modes from T-O-T and O-T-O where T=Si and/or Al [Freeman *et al.*, 2008]. The band below 200 cm^{-1} in labradorite may be a combination of Si-O lattice vibrations with a contribution from larger cations (Me-O in Figure 15) like Ca and Na in the structure [Frogner *et al.*, 1998]. In analcime a band at 3560 cm^{-1} is assigned to O-H stretching of structurally bonded water [Frost *et al.*, 2014]. A similar but much broader band between about 3200 and 3600 cm^{-1} is obtained in the spectrum of chabazite, confirming its presence in vesicles (Figure 15). Both the Raman spectra (Figure 15) and SiO_2 concentration profile (Figure 14) across the ~5 μm boundary layer confirms a transition from labradorite to analcime within this layer.

4.3. Geochemical Modeling

Geochemical modeling of in situ conditions of HA-01 at 68°C using PhreeqC Interactive together with the Iln database suggests that Ca-rich plagioclase, sanidine feldspar, and pyroxene were undersaturated, whereas analcime, Na-Ca-zeolites, and calcite were saturated in groundwater at Hafraflækur for most of the study period. Analcime, Na-Ca-zeolites, and calcite were found in the drill cuttings of HA-04. High Mg,Fe smectite fluctuated between being undersaturated and being saturated throughout most of the study but remained undersaturated after the earthquake on 2 April 2013. These calculations were necessarily limited by availability of reliable thermodynamic data. We used anorthite to represent labradorite, hedenbergite, and a Ca-Al pyroxene to represent augite and a range of zeolites (mesolite, scolecite, laumontite, and natrolite) because reliable thermodynamic data for chabazite and thomsonite are missing from the literature. The database does, however, contain thermodynamic data for smectite, sanidine, stilbite, and analcime. Saturation indices for anorthite, Ca-Al pyroxene, sanidine, analcime, mesolite, scolecite, high Mg,Fe smectite, and calcite are shown in Figure 16.

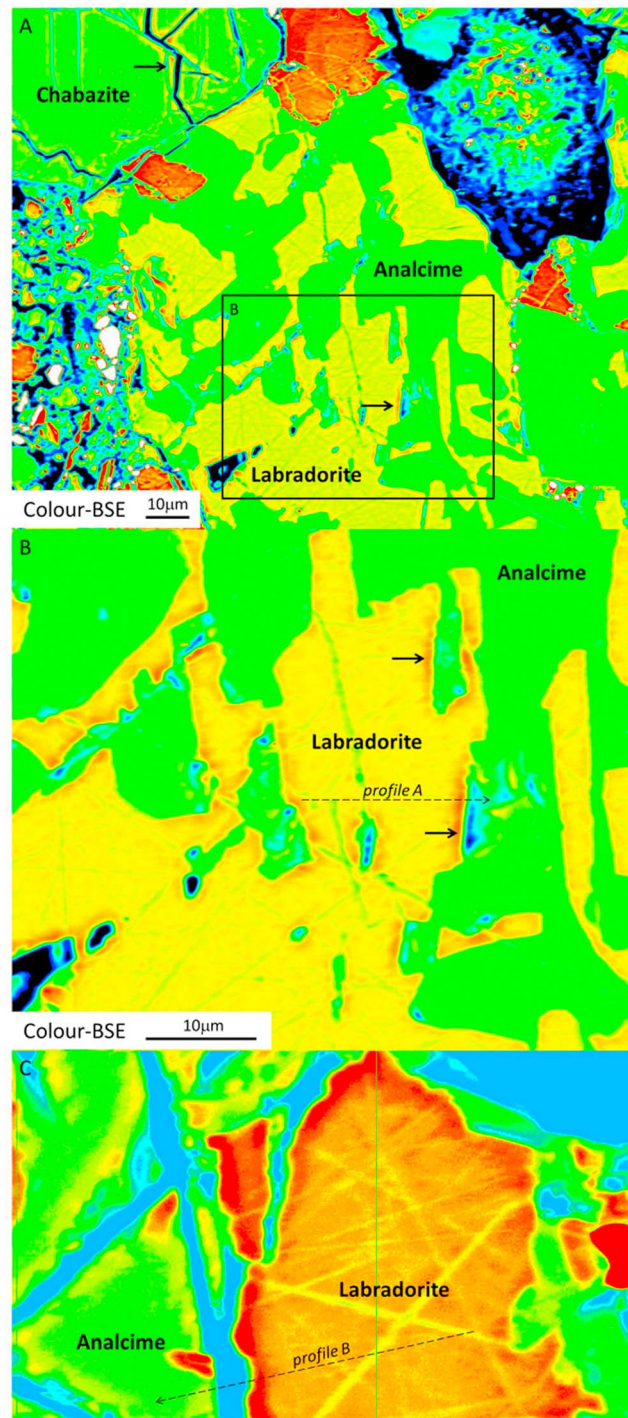


Figure 13. Color-enhanced (BSE) images of area indicated in Figure 11. Figure 13b is a close-up of the area indicated in Figure 11a. The edges of labradorite crystals adjacent to analcime and/or fractures and of chabazite adjacent to fractures show higher atomic densities. The positions of the chemical profiles in Figures 14a and 14b are shown. These images were obtained by EPMA at 15 kV. The color scale is from low (blue and green) to high (yellow and red) atomic density.

5. Discussion

5.1. Long-Term Changes of Groundwater Chemistry

In this section we attempt to relate changes of groundwater chemistry at Hafraalækur from October 2008 to August 2012 (i.e., before the earthquakes) to mineralogical changes seen in drill cuttings from adjacent borehole HA-04. We assume that (1) drill cuttings are representative of the aquifers from which groundwater samples were taken and (2) water-rock interaction is a primary control of groundwater chemistry. Our first assumption is supported by the proximity and similar stratigraphy of the boreholes (Figures 3 and 4). The second assumption is supported by pre-Holocene $\delta^2\text{H}$ values (Figure 5) implying long residence times (>10,000 years).

By far the most striking change in groundwater chemistry before the earthquakes is a steady decrease in the concentrations of Si and Na with a ratio of 2:1 (Figures 4 and 5). There was also a concomitant but order-of-magnitude smaller decrease of Ca concentration and increase of K concentration. There was no statistically significant change of Al concentration during this time period.

The most striking mineralogical change seen in these drill cuttings is illustrated in Figure 10. This figure shows a well-defined inverse correlation between volume percent feldspar and volume percent zeolites ($R^2=0.95$) from which we infer replacement of feldspars (labradorite + sanidine) by analcime and zeolites (chabazite + thomsonite + stilbite + epistilbite + gobbinsite + natrolite).

Figures 11–15 show pseudomorphic replacement of labradorite by analcime, whereas Figure 7 shows that zeolites fill vesicles and fractures. Patchy pseudomorphism with no visible sign of a volume change as well as the narrow ($\sim 5\ \mu\text{m}$) boundary layers between reactant labradorite and product analcime is consistent with replacement by an interface-coupled dissolution-precipitation mechanism [cf. Putnis, 2002]. This would be accompanied by a release of elements into solution and

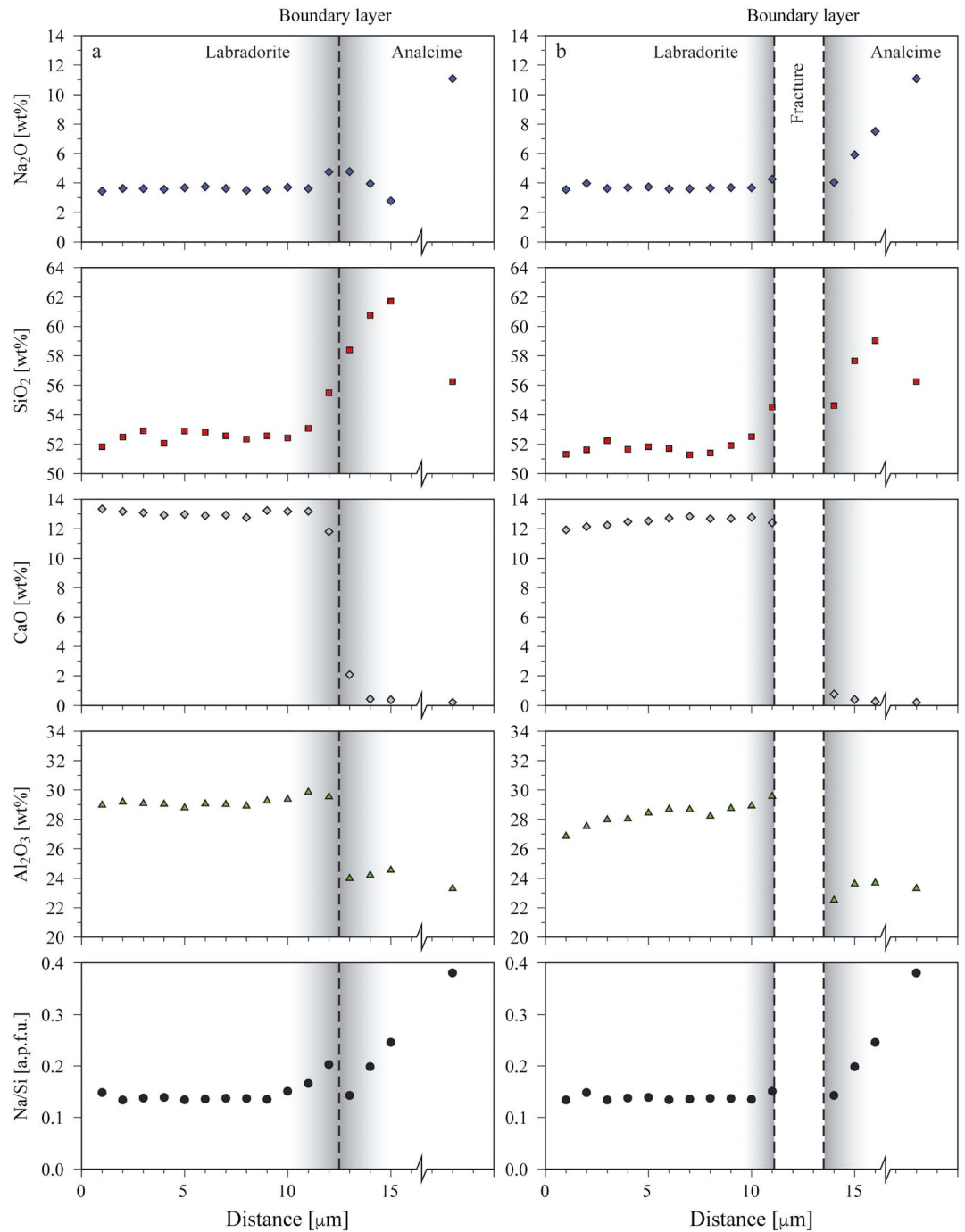


Figure 14. Profiles of Si, Na, Ca, and Al concentration and Na:Si ratio (atoms per formula unit) across (a) unfractured and (b) fractured boundaries between labradorite and analcime from the breccia at a depth of 42 m.

analcime, which was produced would be porous allowing continued fluid access to the reactive interface. Constant volume replacement of 1 mol of labradorite ($\text{Na}_{0.4}\text{Ca}_{0.6}\text{Al}_{1.6}\text{Si}_{2.4}\text{O}_8$) by analcime ($\text{NaAlSi}_2\text{O}_6\text{H}_2\text{O}$) produces 0.4 mol of (porous) analcime and releases 1.6 mol of Si, 1.2 mol of Al, and 0.6 mol of Ca into solution. We would thus expect this replacement reaction on its own to cause an *increase* in the concentrations of Si, Al, and Ca in molar proportions 1.6:1.2:0.6. This was not observed. Instead, we observed a *decrease* in the concentrations of Si and Na in molar proportions 2:1 (Figure 5). This change of groundwater chemistry cannot be explained by constant volume replacement of labradorite by analcime. Precipitation of zeolites observed at

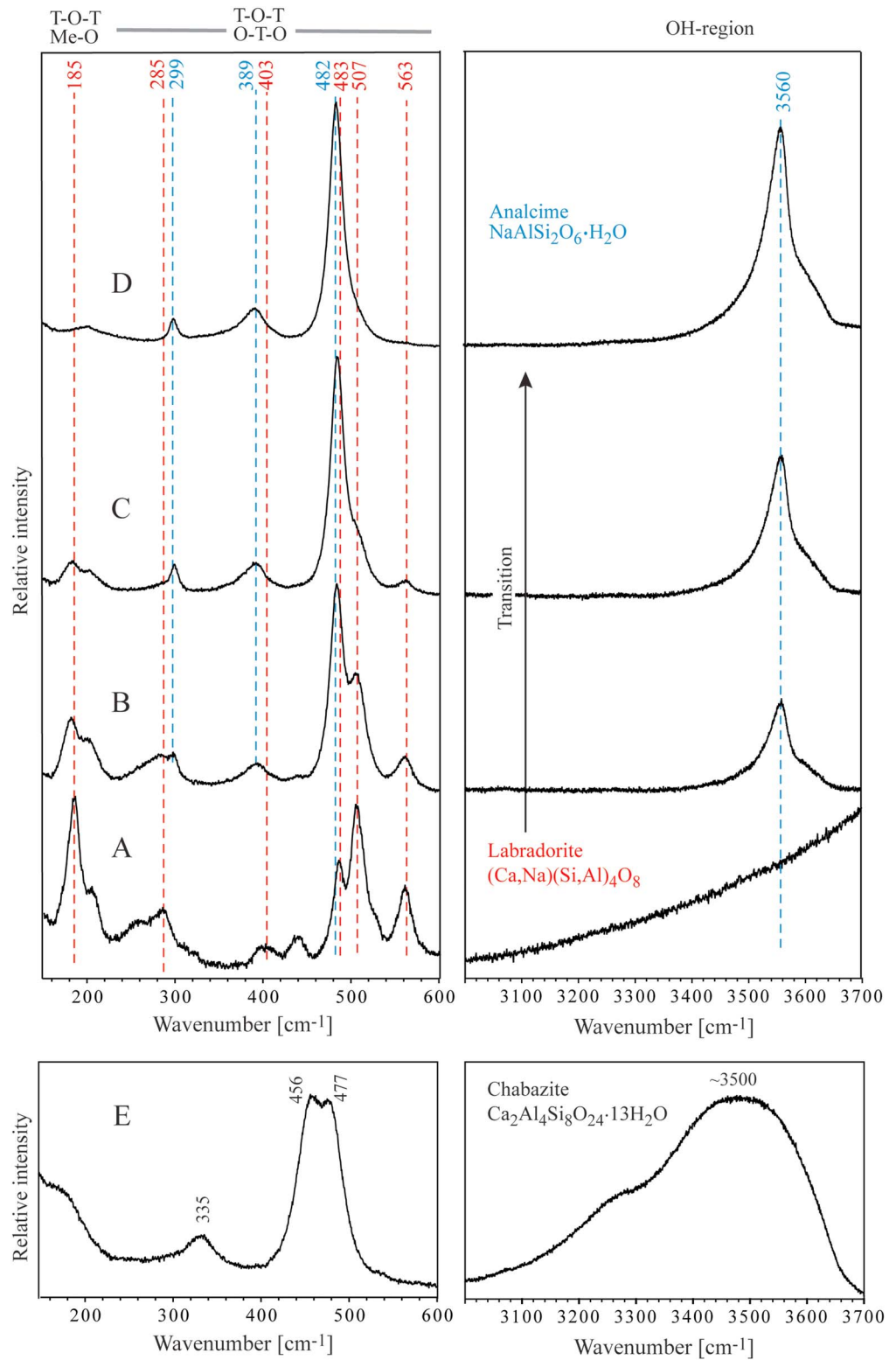


Figure 15. Raman spectra in the spectral range 150–600 cm⁻¹ and 3000–3700 cm⁻¹ of the plagioclase identified as labradorite (A) and the zeolite identified as analcime (D). Peak positions indicated by red numbers are for labradorite and blue for analcime. The spectral range for the T-O-T and O-T-O (T = Si,Al) vibrational region is in the left part and the OH region in the right part. Me-O involves cations like Ca and Na. The two spectra in B and C illustrate the replacement from labradorite to analcime. Spectra A–D were from the boundary as profile A in Figure 13. The spectrum in E is from a separate grain of chabazite.

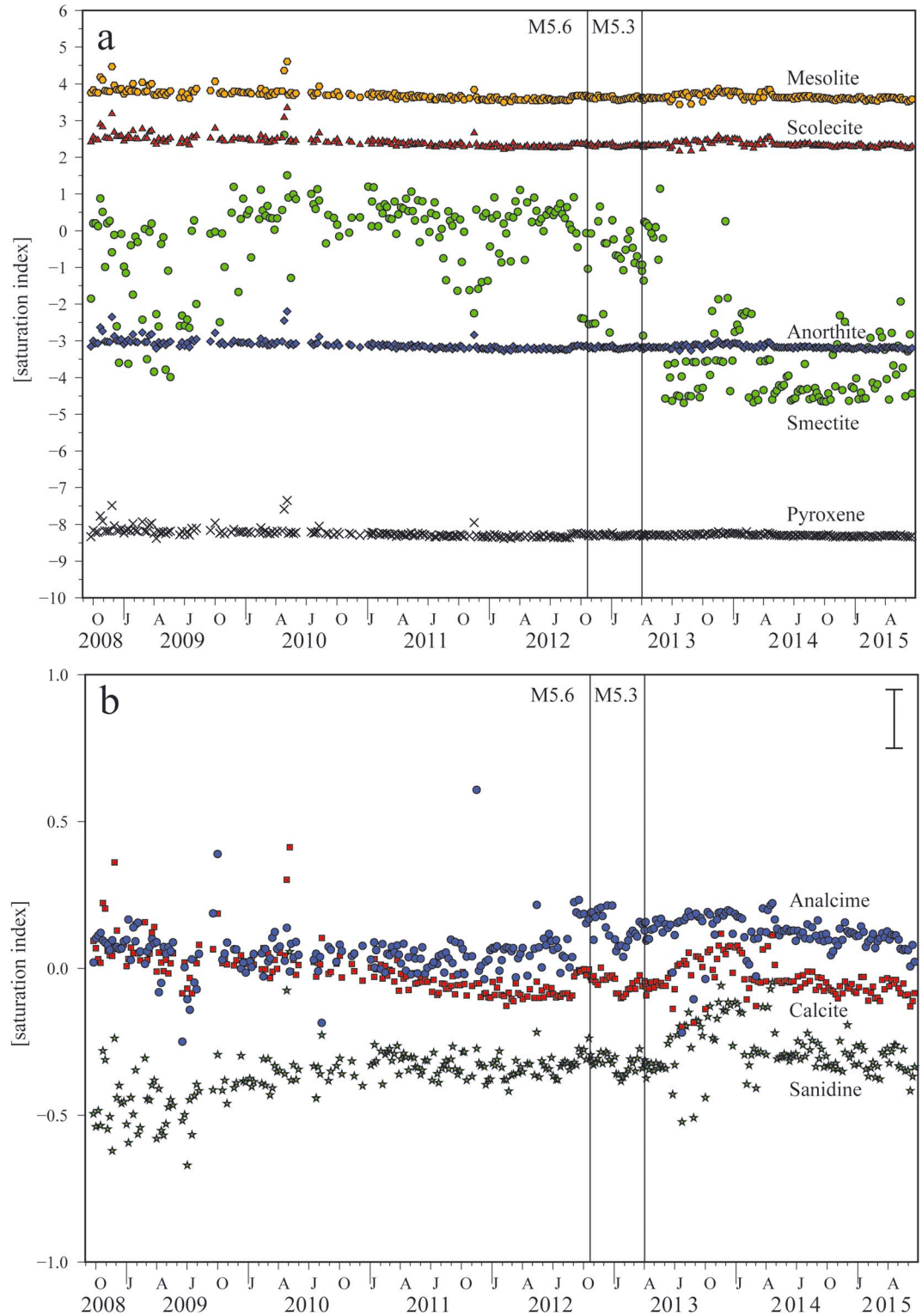


Figure 16. Results of PhreeqC Interactive modeling of in situ conditions of the water chemistry in HA-01 at 68°C for (a) pyroxene, smectite, anorthite, mesolite, and scolecite and (b) analcime, calcite, and sandine. Saturation index is defined as follows: $SI = \log(IAP/K_{sp})$, where IAP is the ion activity product and K_{sp} refers to the solubility product of the solid phase. $SI = 0$ is saturated, $SI < 0$ undersaturated, and $SI > 0$ supersaturated. Minerals sitting on saturation ($SI = 0$) can be indicative of the mineral phase, e.g., analcime and calcite being at water-mineral chemical equilibrium. The uncertainty on SI is estimated to ± 0.10 log units as shown in Figure 16b. The error bars are within the symbols on Figure 16a.

Hafralækur could explain a decrease in concentration of Si and/or Na in groundwater. However, a concomitant decrease in concentration of Al would also be expected. This is not observed. We conclude that *separately*, neither constant volume replacement of labradorite by analcime nor precipitation of zeolites can explain the change of groundwater chemistry seen at Hafralækur. However, we can explain these changes by considering *both* constant volume replacement of labradorite by analcime *and* precipitation of zeolites as follows.

Constant volume replacement of labradorite by analcime causes release of Si, Al, and Ca in molar proportions 1.6:1.2:0.6. The molar ratio of Al and Ca released by this mechanism is therefore 2:1. Several of the zeolites seen at Hafralækur contain Al and Ca in similar stoichiometric proportions (Table 3). Thus, precipitation of one or more of these zeolites could remove Al and Ca in similar or identical proportions to those released by constant volume replacement of labradorite by analcime. Depending on the relative proportions and compositions of these zeolites, Na and/or additional Si is also required for precipitation to occur, and a corresponding decrease in the concentrations of these elements in groundwater is expected. For example, precipitation of epistilbite ($\text{CaAl}_2\text{Si}_6\text{O}_{16}(\text{H}_2\text{O})_5$) and gobbssinite ($\text{Na}_6\text{Ca}_3\text{Al}_6\text{Si}_{10}\text{O}_{32}(\text{H}_2\text{O})_{12}$) in molar proportions 3:1 could explain the observed 2:1 decrease in the concentrations of Si and Na. Precipitation of chabazite ($\text{Ca}_2\text{Al}_4\text{Si}_8\text{O}_{24}(\text{H}_2\text{O})_{13}$) or a higher proportion of epistilbite would increase the molar proportion of Si removed from groundwater, whereas precipitation of a higher proportion of gobbssinite would increase the molar proportion of Na removed from groundwater. Precipitation of thomsonite, stilbite, natrolite, or a different composition of gobbssinite would affect the molar proportions of not only Si and Na but also Ca removed from or added to groundwater.

In summary, we explain chemical changes in groundwater at Hafralækur from October 2008 to August 2012 by a two-stage reaction: constant volume replacement of labradorite by analcime and precipitation of some combination of chabazite, thomsonite, stilbite, epistilbite, gobbssinite, and natrolite in vesicles and/or along fractures.

The validity of this mechanism is further corroborated by geochemical modeling performed using PhreeqC Interactive. The modeling results (Figure 16) show that whereas labradorite (represented by anorthite) and sanidine are undersaturated in groundwater at Hafralækur, analcime is saturated, and the Ca, Na zeolites are oversaturated.

Finally, we have not discussed the small decrease in concentration of Ca and the small increase in concentration of K seen during the same time period. This is because these changes are an order-of-magnitude smaller than observed changes in concentration of Si and Na. The decrease in concentration of Ca probably reflects a slightly higher amount of Ca in one or more of the precipitated zeolites. The increase in the concentration of K in groundwater probably reflects replacement of sanidine as well as labradorite.

5.2. Changes of Groundwater Chemistry Associated With Earthquakes

In this section we attempt to explain changes of groundwater chemistry, which were probably associated (p value = $10^{-5.5}$) with earthquakes on 21 October 2012 and 2 April 2013. The most striking changes were the $\delta^2\text{H}$ and Na maxima, which coincided with these earthquakes [Skelton *et al.*, 2014].

Figure 6 shows that each $\delta^2\text{H}$ maximum began with a gradual increase of $\delta^2\text{H}$ values from slightly less than the baseline value of -126.6 ± 2.7 ‰ reported by Skelton *et al.* [2014]. The first of these increases began at the end of March 2012, 6 months before the first earthquake. The increase was approximately linear with time, reaching a maximum value of -122.0 ± 0.6 ‰ at the end of August 2012, 2 months before the first earthquake. This was followed by a slight decrease to a value of -122.9 ± 0.6 ‰ at the time of the earthquake. The behavior of Na was different. Its concentration increased abruptly at the end of August 2012, 2 months before the first earthquake, from 2588 ± 52 $\mu\text{mol/kg}$ on 28 August to 2794 ± 56 $\mu\text{mol/kg}$ on 3 September 2012. The concentration of Na remained elevated until ~ 2 months after the first earthquake, before decreasing. Similar behavior was seen before the second earthquake. Following the earthquakes, $\delta^2\text{H}$ values and Na concentrations returned to baseline values for the remainder of the study. There is some indication that Si and Ca behaved in a similar manner to Na. However, molar changes were too small to be statistically separable from normal variation [Skelton *et al.*, 2014].

Skelton *et al.* [2014] related the $\delta^2\text{H}$ maxima to preseismic dilation. These authors argued that dilation caused mixing of groundwater components. The observed increase of $\delta^2\text{H}$ before each earthquake could be explained by gradual mixing with modern-day groundwater, which is expected to have less negative $\delta^2\text{H}$

values than the isotopically negative Ice Age groundwater at Hafraalækur. It is, however, unlikely that gradual mixing between this Ice Age groundwater and modern-day groundwater can also explain the Na maxima. This is because these maxima began abruptly and at a different time (2 months rather than 6 months before the first earthquake) than the $\delta^2\text{H}$ maxima. Also, it is unlikely that modern-day groundwater will have higher concentrations of these elements than Ice Age groundwater because modern-day groundwater has had less time to acquire these elements from the host rock. We thus explore alternative causes of the Na maxima that were associated with the earthquakes.

In the previous section, we considered how groundwater chemistry was affected by constant volume replacement of labradorite by analcime and precipitation of zeolites in vesicles and along fractures. These are the only minerals we consider, because no other primary or secondary minerals present in drill cuttings from Hafraalækur contain Na. Also, no basaltic glass (which might contain Na) was found in samples from Hafraalækur. However, neither constant volume replacement of labradorite by analcime, precipitation of zeolites, nor a combination of these mechanisms can explain the increase in concentration of Na observed before the first earthquake for the following reasons:

1. Constant volume replacement of labradorite by analcime releases Si, Al, and Ca, causing an increase in their concentrations. This mechanism cannot, however, explain the observed increase of Na concentration because this element is *not* released into solution.
2. Precipitation of zeolites *removes* some combination of Si, Al, Ca, and/or Na from solution. This mechanism could only explain a decrease not an increase in Na concentration.
3. As described in the previous section, a combination of these processes also removes Si, Na, and/or Ca from solution. Again, because Na is removed, this cannot therefore explain an increase in Na concentration.

In the above cases, we have assumed that dissolution was stoichiometric. Because no reaction pathway can be found, we argue that a switchover to nonstoichiometric dissolution with preferential release of Na occurred 2 months before the first earthquake. The following arguments point to such a switchover having occurred.

1. Figure 5b shows Na concentration plotted against $\delta^{18}\text{O}$ values. There is a positive correlation until August 2012. This implies that Na release was coupled with oxygen isotope exchange between groundwater ($\delta^{18}\text{O}$ range from -18 to -15 ‰) and the host rock ($\delta^{18}\text{O} \geq 5$ ‰). This is consistent with replacement of primary feldspars by secondary zeolites (as described in the previous section) with oxygen isotope exchange occurring during replacement of the primary minerals. From September 2012 onward, no correlation is seen between Na concentration and $\delta^{18}\text{O}$ values. This implies that release of this element from the host rock was not accompanied by oxygen isotope exchange. This could occur either by dissolution of a secondary mineral (a zeolite) which had already acquired its $\delta^{18}\text{O}$ value from groundwater or by nonstoichiometric dissolution of a primary mineral (labradorite). Even in the former case, Na was released preferentially, i.e., dissolution was nonstoichiometric.
2. Mineral chemistry data (Table 2) show that the Na:Si ratio of analcime in breccia clasts from Hafraalækur is lower ($<0.4:1$) than for stoichiometric analcime (0.5:1). This is most extreme alongside fractures (Figure 12) where the Na:Si ratio decreases to 0.14:1. This reflects a decrease in the concentration of Na_2O to ~ 4 wt % (compared with 14.09 wt % for stoichiometric analcime). We argue that this stoichiometric imbalance reflects preferential release of Na into groundwater from analcime, especially alongside fractures. The mechanism whereby this occurs is uncertain, but given that the water content of analcime inferred from EPMA totals (Table 2) is higher (up to 10.43 wt % alongside fractures) than for stoichiometric analcime (8.17 wt %), we infer replacement of Na^+ by hydronium ions (H_3O^+). The lack of a corresponding change in $\delta^{18}\text{O}$ implies that analcime had already acquired its $\delta^{18}\text{O}$ value from groundwater.
3. In a laboratory study of analcime dissolution, which was run at 70°C and pH 10–11, i.e., similar conditions to groundwater at Hafraalækur, *Savage et al.* [2001] showed that release of Na was enhanced by up to a factor of 30 compared to Si and Al.

Based on these corroborating arguments, we propose that preferential release of Na caused by nonstoichiometric dissolution of analcime especially alongside fractures caused the dramatic increase of Na concentration 2 months before the first earthquake.

The switchover from stoichiometric replacement of feldspars by zeolites to nonstoichiometric dissolution of analcime was evidently transient. Figure 5a shows that this switchover caused a shift of the Si:Na ratio from

2:1 in August 2012 to <1:1 at the time of the earthquakes. This ratio recovered gradually after the earthquakes. Peaks of Na concentration and atomic density are seen in labradorite alongside fractured and nonfractured boundaries with analcime (Figures 11 and 12). We suggest that these peaks could record this recovery process, i.e., an uptake of Na from groundwater following the earthquakes. Uptake of Na could have been facilitated by enhanced porosity at these boundaries. Enhanced porosity can be inferred from calculated EPMA totals exceeding 100% (Table 2), which cause the peaks in atomic density (Figures 11 and 12). *Knizek and Jurek* [1994] showed that high EPMA totals can reflect high surface porosity. High boundary layer porosity is further consistent with an interface-coupled precipitation-dissolution mechanism for replacement of labradorite to analcime [cf. *Putnis*, 2002; *Putnis*, 2009].

The reason that a switchover from stoichiometric replacement of feldspars by zeolites to nonstoichiometric dissolution of analcime occurred before each earthquake remains uncertain. Possible triggers include an increase of reactive surface area in contact with groundwater or a shift from water-rock chemical equilibrium.

An increase of reactive surface area could arise due to fracturing associated with preseismic dilation. Dilation was postulated by *Skelton et al.* [2014] as a cause of mixing between groundwater components that led to the $\delta^2\text{H}$ maxima associated with the earthquakes. There is, however, a mismatch in timing. The $\delta^2\text{H}$ increase was gradual and began 6 months before the first earthquake, whereas the switchover to nonstoichiometric dissolution occurred abruptly 2 months before the first earthquake. One possibility is that some threshold fracture area was required for analcime dissolution to take effect. On reaching this threshold, a positive feedback between porosity generation, groundwater access, and continued dissolution was activated, causing the sudden rise in Na concentration.

A shift from water-rock chemical equilibrium could occur in response to mixing between groundwater components causing, for example, a slight change of pH or temperature. This could trigger analcime dissolution, which has been shown experimentally to be highly sensitive to both pH and temperature [*Savage et al.*, 2001]. In this case, the mismatch in timing between groundwater mixing and the switchover to nonstoichiometric dissolution could be due to some threshold shift from chemical equilibrium being required before analcime dissolution took effect. Again, a positive feedback between porosity generation, groundwater access, and continued dissolution could have led to the sudden rise in Na concentration.

Either or a combination of these mechanisms can (1) explain an abrupt switchover from stoichiometric replacement of feldspars by zeolites to nonstoichiometric dissolution of analcime and (2) link this switchover to mixing between groundwater components which *Skelton et al.* [2014] attributed to preseismic dilation. This raises a fundamental question as to why changes of groundwater chemistry apparently coupled with preseismic dilation were seen at Hafralækur, 76 km from the epicenters of two $M > 5$ earthquakes, while geodetic measurements made along the San Andreas Fault, less than 10 km from the epicenter of the $M 6.0$ Parkfield earthquake revealed no evidence of preseismic change of dilational strain [*Johnston et al.*, 2006]. This paradox could be resolved if both chemical changes in groundwater and the earthquakes could be related to magma movement. However, based on geodetic measurements, *Jónsson et al.* [2013] showed that the earthquakes in question were unrelated to magmatism but occurred in response to passive rifting. Also, no hydrochemical response was seen in connection with the recent Holuhraun eruption in Iceland and the associated Bárðarbunga volcano seismicity from August 2014 to February 2015 [*Sigmundsson et al.*, 2014]. We therefore conclude that preseismic dilation remains the most likely cause of chemical changes in groundwater at Hafralækur. The fluctuations of element concentrations and stable isotope ratios seen before the earthquakes compared with more stable values after the earthquakes (Figures 4 and 5) might suggest that whatever process causes dilation acts over a period of years.

6. Conclusion

The concentrations of Si and Na in groundwater collected from a borehole at Hafralækur, northern Iceland, decreased steadily from October 2008 to August 2012. Based on a geochemical and petrological study of drill cuttings from an adjacent borehole, we conclude that this decrease was caused by constant volume replacement of labradorite by analcime coupled with precipitation of zeolites in vesicles and along fractures.

This was followed by an abrupt increase of Na concentration in groundwater, 2 months before the first of two $M > 5$ earthquakes, which occurred in 2012 and 2013, both 76 km from Hafralækur. Based on our petrological

findings, stable isotope data and by comparison with experimental studies, we conclude that this increase was caused by a switchover to nonstoichiometric dissolution of analcime, which led to the preferential release of Na into groundwater. Na concentration peaks coincided with both earthquakes and were followed by a return to preearthquake values as excess Na was taken up along fractured or porous boundaries between labradorite and analcime crystals. We interpret that the Na peaks reflect an increase of reactive surface area caused by fracturing or a shift from chemical equilibrium caused by mixing between groundwater components. In both cases, preseismic dilation is a plausible trigger. A mechanism whereby preseismic dilation can occur, so far, from the focus of an earthquake remains to be discovered.

Acknowledgments

We would like to thank the reviewers Steve Ingebritsen and Monica Piochi for their valuable comments, which greatly improved the manuscript. Our most sincere thanks go to Berndt Nyberg for assistance during fieldwork and general support. Dan Zetterberg is thanked for sample preparation at Stockholm University. The Icelandic Metrological Office is thanked for the earthquake data. Financial support from the Swedish Research Council is gratefully acknowledged. All data are available from Alasdair Skelton, Stockholm University (Alasdair.Skelton@geo.su.se).

References

- Árnason, B. (1977), Hydrothermal systems in Iceland traced by deuterium, *Geothermics*, *5*, 125–151.
- Claesson, L., A. Skelton, C. Graham, C. Dietl, C.-M. Mörth, P. Torssander, and I. Kockum (2004), Hydrochemical changes before and after a major earthquake, *Geology*, *32*, 641–644.
- Claesson, L., A. Skelton, C. Graham, and C.-M. Mörth (2007), The timescale and mechanisms of fault sealing and water-rock interaction after an earthquake, *Geofluids*, *7*, 427–440.
- Downs, R. T. (2006), The RRUFF Project: An integrated study of the chemistry, crystallography, Raman and infrared spectroscopy of minerals, *Program and Abstracts of the 19th General Meeting of the International Mineralogical Association in Kobe, Japan, 003-13*.
- Einarsson, P., and K. Sæmundsson (1987), Earthquake epicenters 1982–1985 and volcanic systems in Iceland, in *Í hlutarins eðli: Festschrift for Thorbjörn Sigurgerirsson*, edited by T. Sigfússon, Menningarsjóður, Reykjavík.
- Freeman, J. J., A. Wang, K. E. Kuebler, B. L. Jolliff, and L. A. Haskin (2008), Characterization of natural feldspars by Raman spectroscopy for further planetary exploration, *Can. Mineral.*, *46*, 1477–1500.
- Friðleifsson, G. Ó. (1997), Hafralækur, Hóla 4, Orkustofnun Rep. GÖF-97/01.
- Frogner, P., C. Broman, and S. Lindblom (1998), Weathering detected by Raman spectroscopy using Al-ordering in albite, *Chem. Geol.*, *151*, 161–168.
- Frost, R. L., A. López, F. L. Theiss, A. Wilson Romano, and R. Scholz (2014), A vibrational spectroscopic study of the silicate mineral analcime $\text{Na}_2(\text{Al}_4\text{SiO}_4\text{O}_{12})\cdot\text{H}_2\text{O}$ —A natural zeolite, *Spectrochim. Acta A Mol. Biomol. Spectrosc.*, *133*, 521–525.
- Govindaraju, K. (1994), 1994 compilation of working values and sample description for 383 geostandards, *Geostand. Newsl.*, *18*(special issue), 158.
- Hauksson, E., and J. G. Goddard (1981), Radon earthquake precursor studies in Iceland, *J. Geophys. Res.*, *86*(B8), 7037–7054, doi:10.1029/JB086iB08p07037.
- Igarashi, G., S. Saeki, N. Takahata, K. Sumikawa, S. Tasaka, Y. Sasaki, M. Takahashi, and Y. Sano (1995), Ground-water radon anomaly before the Kobe earthquake in Japan, *Science*, *269*, 60–61.
- Ingebritsen, S., and M. Manga (2014), Earthquakes: Hydrogeochemical precursors, *Nat. Geosci.*, *7*, 697–698.
- Johannesson, H., and K. Sæmundsson (2009), Geological map of Iceland. 1:600 000 bedrock geology, Icelandic Institute of Natural History, Reykjavík (1st edition).
- Johnston, M. J. S., R. D. Borcherdt, A. T. Linde, and M. T. Gladwin (2006), Continuous borehole strain and pore pressure in the near field of the 28 September 2004 M 6.0 Parkfield, California, earthquake: Implications for nucleation, fault response, earthquake prediction, and tremor, *Bull. Seismol. Soc. Am.*, *96*, S56–S72.
- Jónsson, S., S. Metzger, S. Hreinsdóttir, E. Rivalta, L. Passarelli, and F. Maccaferri (2013), The 2012–2013 earthquake sequences in North Iceland: Geodetic constraints and associated stress changes, *Proceedings of the International Workshop on Earthquakes in North Iceland, Húsavík, North Iceland, 6–8 June 2013*, 74–77.
- Knizek, K., and K. Jurek (1994), Correction procedure for the electron microprobe analysis of porous materials, *Microchim. Acta*, *117*, 87–93.
- Kristmannsdóttir, H., S. Arnórsson, A. E. Sveinbjörnsdóttir, and H. Ármannsson (2010), Chemical variety of water in Icelandic heating systems. *Proceedings of the World Geothermal Congress 2010*, 1477, 1–9.
- Larsson, D., K. Grönvold, N. Oskarsson, and E. Gunnlaugsson (2002), Hydrothermal alteration of plagioclase and growth of secondary feldspar in the Hengill Volcanic Centre, SW Iceland, *J. Volcanol. Geotherm. Res.*, *114*, 275–290.
- Norrish, K., and J. T. Hutton (1969), An accurate X-ray spectrographic method for the analysis of a wide range of geological samples, *Geochim. Cosmochim. Acta*, *33*, 431–453.
- Ólafsson, M. (2011), Orkuveita Húsavíkur Efnavöktun 2007 og 2010, ISOR-2011/004 Rep., 21 pp.
- Parkhurst, D. L., and C. A. J. Appelo (1999), User's guide to PHREEQC (version 2)—A computer program for speciation, batch-reactions, one-dimensional transport, and inverse geochemical calculations, *U.S. Geol. Surv. Water Resour. Invest. Rep.* 99-4259.
- Pearce, J. A., and M. J. Norry (1979), Petrogenetic implications of Ti, Zr, Y, and Nb variations in volcanic rocks, *Contrib. Mineral. Petrol.*, *69*, 33–47.
- Putnis, A. (2002), Mineral replacement reactions: From macroscopic observations to microscopic mechanisms, *Min. Mag.*, *66*, 689–708.
- Putnis, A. (2009), Mineral replacement reactions, *Rev. Mineral. Geochem.*, *70*, 87–124.
- Reddy, D., P. Nagabhushanam, and B. S. Sukhija (2011), Earthquake (M 5.1) induced hydrogeochemical and $\delta^{18}\text{O}$ changes: Validation of aquifer breaching—Mixing model in Koyna, India, *Geophys. J. Int.*, *184*, 359–370.
- Riedel, C., A. Tryggvason, T. Dahm, R. Stefansson, R. Bóðvarsson, and G. B. Gudmundsson (2005), The seismic velocity structure north of Iceland, *J. Seismol.*, *5*, 383–404.
- Rietveld, H. (1969), A profile refinement method for nuclear and magnetic structures, *J. Appl. Crystallogr.*, *2*, 65–71, doi:10.1107/S0021889869006558.
- Roeloffs, E. (1988), Hydrologic precursors to earthquakes: A review, *Pure Appl. Geophys.*, *126*, 177–209.
- Sæmundsson, K. (1991), Jarðfræði Kröflukerfisins, in *Náttúra Mývatns*, edited by A. Gardarsson and Á. Einarsson, pp. 24–95, Hið Íslenska Náttúrufræðifélag, Reykjavík.
- Sæmundsson, K., and E. Gunnlaugsson (2014), Icelandic rocks and minerals, Forlagid ehf, Reykjavík 2014.
- Savage, D., C. Rochelle, Y. Moore, A. Milodowski, K. Bateman, D. Bailey, and M. Mihara (2001), Analcime reactions at 25–90°C in hyperalkaline fluids, *Min. Mag.*, *65*, 571–587.
- Scholz, C. H., L. R. Sykes, and Y. P. Aggarwal (1973), Earthquake prediction: A physical basis, *Science*, *181*, 803–810.

- Sigmundsson, F., et al. (2014), Segmented lateral dyke growth in a rifting event at Bárðarbunga volcanic system, Iceland, *Nature*, *517*, 191–195.
- Sigurðsson, F. (1965), Jarðviðnámsmælingar Sumarið 1964, Raforkumálastjóri Jarðhitadeild, Reykjavík.
- Skelton, A., et al. (2014), Changes in groundwater chemistry before two consecutive earthquakes in Iceland, *Nat. Geosci.*, *7*, 752–756.
- Song, S., et al. (2006), Hydrogeochemical anomalies in the springs of the Chiayi area in west-central Taiwan as possible precursors to earthquakes, *Pure Appl. Geophys.*, *163*, 675–691.
- Stefánsson, A., S. R. Gíslason, and S. Arnórsson (2001), Dissolution of primary minerals in natural waters II. Mineral saturation state, *Chem. Geol.*, *172*, 251–276.
- Stefánsson, R., G. B. Gudmundsson, and P. Halldorsson (2008), Tjörnes Fracture Zone. New and old seismic evidences for the link between the North Atlantic rift zone and the Mid-Atlantic ridge, *Tectonophysics*, *447*, 117–126.
- Sveinbjörnsdóttir, Á. E., H. Ármannson, M. Ólafsson, F. Óskarsson, S. Markússon, and S. Magnúsdóttir (2013), The Theistareykir geothermal field, NE Iceland. Isotopic characteristics and origin of circulating fluids, *Procedia Earth Planet. Sci.*, *7*, 822–825.
- Thomas, D. (1988), Geochemical precursors to seismic activity, *Pure Appl. Geophys.*, *126*, 241–266.
- Tsunogai, U., and H. Wakita (1995), Precursory chemical changes in ground water: Kobe earthquake, Japan, *Science*, *269*, 61.
- Wakita, H. (1981), Precursory changes in groundwater prior to the 1978 Izu-Oshima-Kinkai earthquake, in *Earthquake Prediction*, edited by D. W. Simpson and P. G. Richards, AGU, Washington, D. C., doi:10.1029/ME004p0527.
- Wakita, H. (1996), Geochemical challenge to earthquake prediction, *Proc. Natl. Acad. Sci. U.S.A.*, *93*, 3781–3786.
- Wakita, H., G. Igarashi, and K. Notsu (1991), An anomalous radon decrease in groundwater prior to an M6.0 earthquake: A possible precursor? *Geophys. Res. Lett.*, *18*, 629–632, doi:10.1029/91GL00824.
- Wang, C.-Y., and M. Manga (2010), *Earthquakes and Water*, vol. 114, Springer, Berlin, doi:10.1007/978-3-642-00810-8.
- Wästeby, N., A. Skelton, E. Tollefsen, M. Andrén, G. Stockmann, L. Claesson Liljedahl, E. Sturkell, and M. Mörtz (2014), Hydrochemical monitoring, petrological observation, and geochemical modeling of fault healing after an earthquake, *J. Geophys. Res. Solid Earth*, *119*, 5727–5740, doi:10.1002/2013JB010715.
- Weis, F. A., H. Skogby, V. R. Troll, F. M. Deegan, and B. Dahren (2015), Magmatic water contents determined through clinopyroxene: Examples from the Western Canary Islands, Spain, *Geochem. Geophys. Geosyst.*, *16*, 2127–2146, doi:10.1002/2015GC005800.
- Yaman, M., A. Sasmaz, G. Kaya, M. Ince, N. M. Karaaslan, C. Ozcan, and S. Akkus (2011), Determination of elements in thermal springs for monitoring pre-earthquake activities by ICP-MS, *At. Spectrosc.*, *32*, 182–188.